

# Meet-in-the-Middle Attack on Primitives with Binary Matrix Linear Layer

Qingliang Hou<sup>1</sup>, Kuntong Li<sup>1</sup>, Guoyan Zhang<sup>1,2</sup>(✉), Yanzhao Shen<sup>2</sup>,  
Qidi You<sup>3,4</sup>, and Xiaoyang Dong<sup>5</sup>

<sup>1</sup> School of Cyber Science and Technology, Shandong University, Qingdao, China  
{qinglianghou, likuntong}@mail.sdu.edu.cn, guoyanzhang@sdu.edu.cn

<sup>2</sup> Shandong Institute of Blockchain, Jinan, China  
shenyanzhao@sdibc.cn

<sup>3</sup> State Key Laboratory of Space-Ground Integrated Information Technology  
youqd@spacestar.com.cn

<sup>4</sup> Space star Technology Co., Ltd

<sup>5</sup> Institute for Network Sciences and Cyberspace, BNRist, Tsinghua University,  
Beijing, China  
xiaoyangdong@tsinghua.edu.cn

**Abstract.** Meet-in-the-middle (MitM) is a powerful approach for the cryptanalysis of symmetric primitives. In recent years, MitM has led to many improved records about key recovery, preimage and collision attacks with the help of automated tools. However, most of the previous work target AES-like hashing where the linear layer is an MDS matrix. And we observe that their automatic model for MDS matrix is not suitable for primitives using a binary matrix as their linear layer.

In this paper, we propose the  $n$ -XOR model to describe the XOR operation with an arbitrary number of inputs. And it can be applied to primitives with a binary matrix of arbitrary size. Then, we propose a check model to eliminate the possible inaccuracies caused by  $n$ -XOR. But the check model is limited by the input size (not greater than 4). Combined with the two new models, we find a MitM key recovery attack on 11-round Midori64. When the whitening keys are excluded, a MitM key recovery attack can be mounted on the 12-round Midori64. Compared with the previous best work, both of the above results have distinct advantages in terms of reducing memory and data complexity. At last, we apply the  $n$ -XOR model to the hashing modes of primitives with large size binary matrix. The preimage attack on weakened Camellia- $MMO$  (without  $FL/FL^{-1}$  and whitening layers) and Aria-DM are both improved by 1 round.

**Keywords:** Meet-in-the-Middle · Binary Matrix · Key Recovery · Preimage · Midori64 · Camellia · Aria.

---

First Author and Second Author contributed equally to this work.

## 1 Introduction

The Meet-in-the-middle (MitM) is a powerful cryptanalysis strategy first proposed by Diffie and Hellman to attack Double DES [12]. The core idea is to identify two disjoint neutral sets of unknown values. Then, the whole computation path can be divided into two independent chunks, which are determined by two neutral sets and denoted by *forward chunk* and *backward chunk*, respectively. At last, the two chunks will meet at a common internal state where the consistency is checked to filter out candidate assignments of unknown values. From then on, MitM and its variants have been successfully applied to many block ciphers [9,32,18,29]. At SAC 2008, Aumasson *et al.* [3] first introduced the theory of MitM into preimage attacks on step-reduced MD5 and 3-pass HAVAL. Sequentially, many refined techniques were proposed to enhance the power of MitM, such as splice-and-cut [2], initial structure [30], bicliques [8], and so on. At FSE 2011, Sasaki [26] applied such MitM preimage attack to the PGV [25] hashing modes of AES and presented the first preimage attack on 7-round AES-MMO/MP/DM together with the partial indirect matching technique. Interestingly, these enhancements were finally found to be applicable in the key recovery attack on block ciphers. At ACISP 2011, Wei *et al.* [37] broke the full round KTANTAN using the splice-and-cut technique by connecting the plaintext and ciphertext with encryption or decryption oracles with only 4 chosen plaintexts.

Despite being clear that a MitM attack is entirely determined by its *characteristic*, i.e., the configuration for two chunks, it's still complicated and error-prone to explore the whole configuration space. Recently, automated tools were introduced to find the best characteristic by solving an optimization problem. At Eurocrypt 2021, Bao *et al.* [6] proposed an MILP-based MitM preimage attack on AES-like hash and Haraka v2. At CRYPTO 2021, Dong *et al.* [13] extended the automatic model into key-recovery and collision attacks and introduced a table-based method to solve the non-linear constraints imposed on neutral sets. At CRYPTO 2022, Bao *et al.* [7] considered the MitM attack in a view of superposition (SupP) states and bi-directional attribute propagation (BiDir) such that neutral sets are treated independently and can be imposed constraints in both computation paths. At Asiacrypt 2023, Hou *et al.* [17] introduced the SupP framework into Feistel-based hash functions. At Eurocrypt 2024, Chen *et al.* [10] considered the linearization of the S-Box in AES and allowed a linear combination of two neutral sets in the initial structure. Different from the above work, Schrottenloher and Stevens [33] studied a simple top-down modeling paradigm for both classical and quantum preimage attacks against permutations and was later extended to key recovery attack on block ciphers with simple key schedules [34]. The simplified attack excluded many details. In this paper, we adopt the bottom-up MitM framework in [7] and the table-based method in [13].

In the previous work, the targets are most built by a block cipher with an MDS matrix. Through the diffusion layer, each output cell is related to all the input cells. However, the primitives with binary matrix are rarely studied, where each output cell is represented as the XOR of partial input cells. In [13], Dong *et al.* introduced the 3-XOR model for SKINNY- $n-3n$ . In their model, the number

83 of input cells is fixed to be 4. All valid cases can be easily exhausted to form a  
84 system of inequalities using the convex hull method [36]. However, if more input  
85 cells are involved, the number of valid cases will increase extremely leading to  
86 larger size of system of inequalities, which can make model infeasible to compute.  
87 Hence, there is a gap to find an accurate and effective method to describe the  
88 MitM attribute propagation through a binary matrix of arbitrary size.

89 **Our Contributions.** In this paper, we propose a novel model called **n-XOR** un-  
90 der the encoding scheme in [7], to describe the propagation of MitM attributes  
91 through an XOR operation with an arbitrary number of input cells. And the  
92 number of inequalities formed by **n-XOR** is fixed, independent of the number of  
93 inputs. Hence, **n-XOR** can be applied to large binary matrices effectively. How-  
94 ever, we also observe that only applying **n-XOR** will lead to subtle inaccuracies.  
95 An extremely explicit case is that the constraint on the same neutral bits may  
96 be double counted in two different **n-XOR** operations. Besides, there are more  
97 implicit cases depending on the specific linear layer. Hence, we propose an addi-  
98 tional check model to eliminate these inaccuracies. But this model is limited by  
99 the input size  $n$ , that is,  $n \leq 4$  in our paper.

100 As a low-energy lightweight cryptography, **Midori** [5] is well-suited for con-  
101 strained environments, like the edge gateways and end devices in the blockchain  
102 on-chain and off-chain interactions. As a proof of work, we first apply the two  
103 new models to **Midori64** [5], with a  $4 \times 4$  binary matrix as linear layer. Then,  
104 an 11-round key recovery attack is found with time complexity of  $2^{124}$ . The  
105 data and memory complexity are  $2^{36}$  and  $2^6$ , respectively. When omitting the  
106 whitening layer, a 12-round MitM characteristic for weakened **Midori64** is found  
107 with time complexity of  $2^{120}$ . The data and memory cost are  $2^{48}$  and  $2^{10.6}$ , re-  
108 spectively. Besides, the data and memory complexity can be further reduced if  
109 the time complexity is relaxed to  $2^{124}$ . Compared to the previous best records  
110 of **Midori64** [23,35,22], despite a little higher time complexity, our results have  
111 distinct advantages in reducing data and memory complexity.

112 It's a practical design strategy to build hash functions on widely used block  
113 cipher with a longstanding record of cryptanalysis. And **AES-MMO** was even inter-  
114 nationally standardized by ISO [19]. Since **Camellia** [1] was also standardized by  
115 ISO [20] and **Aria** [21] was standardized by Korean Standard (KS X1213), the  
116 hashing modes of **Camellia** or **Aria** may be potential candidates used in prac-  
117 tice. Indeed, their security have been evaluated in a series of works [31,27,16,4].  
118 In this paper, we apply the **n-XOR** to describe the MitM attributes propaga-  
119 tion through the large binary matrix of **Camellia** and **Aria**. Finally, we find a  
120 preimage attack on 14-round weakened **Camellia-MMO** (without  $FL/FL^{-1}$  and  
121 whitening layers) and a preimage attack on 6-round **Aria-DM**. Compared to the  
122 previous best records [28,16], the attack rounds are both improved by 1 round.

123 Our results are also summarized in Table 1 and Table 2. For the source code,  
124 please refer to <https://github.com/wenny-kt/MITM-Binary-Matrix>.

125 The rest of this paper is organized as follows. In Section 2, we give an overview  
126 of how the automated MitM attacks are deployed, along with some enhanced

Table 1: Single Key attacks on Midori64, where ID and  $\mathcal{DS}$ -MitM denote impossible differential and Demirci-Selçuk MitM attack, respectively.

Target	Rounds	Data	Memory(Bytes)	Time(Enc.)	Technique	Ref.
Midori64	11	$2^{60}$	$2^{95.8}$	$2^{116.6}$	ID	[23]
	11	$2^{53}$	$2^{92.2}$	$2^{122}$	$\mathcal{DS}$ -MitM	[22]
	11	$2^{36}$	$2^6$	$2^{124}$	MitM	Section 4.1
	12	$2^{55.5}$	$2^{109}$	$2^{125.5}$	$\mathcal{DS}$ -MitM	[22]
	12 <sup>†</sup>	$2^{61.9}$	$2^{44}$	$2^{90.5}$	ID	[35]
	12 <sup>†</sup>	$2^{48}$	$2^{10.6}$	$2^{120}$	MitM	Section 4.2
	12 <sup>†</sup>	$2^{36}$	$2^{5.6}$	$2^{124}$	MitM	Section 4.2

† Weakened version without whitening layers.

Table 2: A Summary of the MitM Attacks on Hashing Modes.

Target	Attacks	Rounds	Time1	Time2	Memory	Technique	Ref.
Camellia-MMO	Preimage	13 <sup>‡</sup>	$2^{120}$	$2^{125}$	$2^8$	MitM	[28]
		14 <sup>‡</sup>	$2^{120}$	$2^{125}$	$2^8$	MitM	Section 5
Aria-DM	Preimage	5	$2^{120}$	$2^{125}$	$2^8$	MitM	[16]
		6	$2^{120}$	$2^{125}$	$2^{112}$	MitM	Section 6

‡ Weakened version without  $FL/FL^{-1}$  and whitening layers.

\* Time1 represents the time complexity of pseudo-preimage. Time2 represents the time complexity of preimage attack converted from the pseudo-preimage attack according to [24, Fact9.99].

127 techniques. In Section 3, we introduce two new improved models embedded in the  
 128 automated MitM framework, called n-XOR and check model. The applications  
 129 to Midori64, Camellia-MMO and Aria-DM are presented in Sects. 4, 5 and 6,  
 130 respectively. Finally, we conclude in Section 7.

## 131 2 Preliminaries: Automated Meet-in-the-Middle Attack

132 In this section, we provide an overview of how the MitM attack framework is  
 133 constructed, and how it is encoded into the MILP language with specified config-  
 134 urations for the preimage and key recovery attack. Then, we recall two enhanced  
 135 techniques to improve the power of MitM attack. The first one is the *table-based*  
 136 *method* introduced in [13] to solving the non-linear constraints. Another one is  
 137 the *Superposition (SupP) States and Bi-direction Attribute-Propagation (BiDir)*  
 138 introduced in [7] to preserving more valid solutions.

### 139 2.1 Framework of the Meet-in-the-Middle Attack

140 The MitM attack framework is illustrated in Figure 1.  $\mathcal{S}^{\text{ENC}}$  and  $\mathcal{S}^{\text{KEY}}$  are the  
 141 starting states where there are  $\lambda_{\mathcal{B}}^{\text{ENC}}$  and  $\lambda_{\mathcal{B}}^{\text{KEY}}$  neutral bits for forward compu-  
 142 tation denoted by ■, and there are  $\lambda_{\mathcal{R}}^{\text{ENC}}$  and  $\lambda_{\mathcal{R}}^{\text{KEY}}$  neutral bits for backward  
 143 computation denoted by ■. After imposing  $l_{\mathcal{R}}^{\text{ENC}}$  and  $l_{\mathcal{R}}^{\text{KEY}}$  constraints on  $\lambda_{\mathcal{R}}^{\text{ENC}}$  and  
 144  $\lambda_{\mathcal{R}}^{\text{KEY}}$  backward neutral bits, respectively, ■ can be propagated to the matching

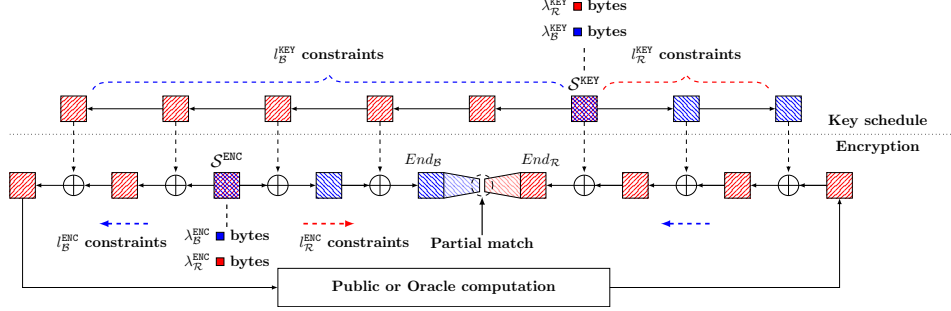


Fig. 1: A high-level overview of the MITM attacks [13]

145 points  $End_B$  independent of the ■ bits. The degree of freedom (DoF) for the ■  
 146 neutral space is computed by  $d_R = \lambda_R^{ENC} + \lambda_R^{KEY} - l_R^{ENC} - l_R^{KEY}$ . Similarly, forward  
 147 neutral bits are imposed on  $l_B^{ENC}$  and  $l_B^{KEY}$  constraints to cancel the effect of ■  
 148 in the backward computation. The DoF of the ■ neutral space can be computed  
 149 by  $d_B = \lambda_B^{ENC} + \lambda_B^{KEY} - l_B^{ENC} - l_B^{KEY}$ . Through a feed-forward mechanism or querying  
 150 a public Encryption-Decryption oracle,  $End_R$  can be derived by ■. Instead of  
 151 requiring the full states, the partial matching exploits the filtering ability derived  
 152 by the deterministic relation “ $End_B = End_R$ ” and denoted by  $d_m$ .

153 With the configurations of  $(\lambda_B^{ENC}, \lambda_B^{KEY}, \lambda_R^{ENC}, \lambda_R^{KEY}, l_B^{ENC}, l_B^{KEY}, l_R^{ENC}, l_R^{KEY}, d_m)$ , the  
 154 basic attack procedure goes as follows:

- 155 1. Choose constants in  $\mathcal{S}^{ENC}$  and  $\mathcal{S}^{KEY}$  and  $l_B^{ENC} + l_B^{KEY} + l_R^{ENC} + l_R^{KEY}$  constraints.
- 156 2. For  $2^{d_B}$  values of ■ neutral space, compute forward to  $End_B$  from the starting  
 157 states, and store the values of ■ in table  $L_B[End_B]$ .
- 158 3. For  $2^{d_R}$  values of ■ neutral space, compute backward to  $End_R$  from the  
 159 starting states, and store the values of ■ in table  $L_R[End_R]$ .
- 160 4. According to the indices, check the match between  $L_B$  and  $L_R$ .
- 161 5. For the surviving pairs that pass the match, check for a full-state match.

162 *Complexity analysis.* The above steps 2-5 form a MitM *episode*. To find an  $h$ -bit  
 163 full match,  $2^{h-(d_B+d_R)}$  episodes are needed. Since each episode is performed with  
 164 a time of  $2^{\max\{d_B, d_R\}} + 2^{d_B+d_R-d_m}$ , the total time complexity is:

$$2^{h-(d_B+d_R)} \cdot (2^{\max\{d_B, d_R\}} + 2^{d_B+d_R-d_m}) \approx 2^{h-\min\{d_B, d_R, d_m\}} \quad (1)$$

165 Apparently, a MitM characteristic is valid, if and only if  $\min\{d_B, d_R, d_m\} \geq$   
 166 1. For MitM key recovery attack, additional constraints must be fulfilled to  
 167 ensure that the internal states in  $\mathcal{S}^{ENC}$  can be totally determined by  $\mathcal{S}^{KEY}$ . This is  
 168 equivalent to using up the DoFs of  $\mathcal{S}^{ENC}$ , i.e.,  $\lambda_B^{ENC} - l_B^{ENC} = 0$  and  $\lambda_R^{ENC} - l_R^{ENC} = 0$ .  
 169 Besides, there should exist only one type of neutral bit in the plaintext or  
 170 ciphertext, and at least 1-bit constant in the plaintext or ciphertext to avoid  
 171 using up the full codebook. In [6], Bao *et al.* encoded the type of each byte in  
 172 AES with a pair of boolean variables:

- 173 1.  $\blacksquare \mathcal{R}, (x, y) = (0, 1)$ : Known byte only with backward computation.
- 174 2.  $\blacksquare \mathcal{B}, (x, y) = (1, 0)$ : Known byte only with forward computation.
- 175 3.  $\blacksquare \mathcal{G}, (x, y) = (1, 1)$ : Constant byte and known in both forward and backward
- 176     computations.
- 177 4.  $\square \mathcal{W}, (x, y) = (0, 0)$ : Unknown byte in forward and backward computations.

178 Then, the propagation rules for XOR and MixColumns can be described as a  
 179 system of inequalities based on the above definitions. A valid MitM characteristic  
 180 is defined as a solution solved by the off-the-shelf MILP solvers, like Gurobi [15],  
 181 with the objective function that maximizes the  $\min\{d_{\mathcal{B}}, d_{\mathcal{R}}, d_m\}$ . For the detailed  
 182 MILP models of these propagation rules, please refer to [6] or Appendix A.

## 183 2.2 Enhanced Techniques

184 **Table-based method solving non-linear constraints.** Note that Equation  
 185 (1) holds mostly when the constraints imposed on neutral bits can be solved  
 186 in  $O(1)$  time, such as linear equations. However, there are many practice MitM  
 187 characteristics with non-linear constrained neutral bits, which can not be solved  
 188 efficiently. In [13], Dong *et al.* proposed a precomputation method to compute  
 189 the value of the constraints by enumerating the neutral bits. Specifically, after  
 190 setting the value of constants in starting states, do as follows:

- 191 1. For  $2^{\lambda_{\mathcal{B}}^{\text{ENC}} + \lambda_{\mathcal{B}}^{\text{KEY}}}$   $\blacksquare$  values, compute the values of  $l_{\mathcal{B}}^{\text{ENC}} + l_{\mathcal{B}}^{\text{KEY}}$  constraints (denoted  
 192     by  $\mathbf{c}_{\mathcal{B}} \in \mathbb{F}_2^{l_{\mathcal{B}}^{\text{ENC}} + l_{\mathcal{B}}^{\text{KEY}}}$ ) and store the  $\lambda_{\mathcal{B}}^{\text{ENC}} + \lambda_{\mathcal{B}}^{\text{KEY}}$   $\blacksquare$  bits in  $U[\mathbf{c}_{\mathcal{B}}]$ .
- 193 2. For  $2^{\lambda_{\mathcal{R}}^{\text{ENC}} + \lambda_{\mathcal{R}}^{\text{KEY}}}$   $\blacksquare$  values, compute the values of  $l_{\mathcal{R}}^{\text{ENC}} + l_{\mathcal{R}}^{\text{KEY}}$  constraints (denoted  
 194     by  $\mathbf{c}_{\mathcal{R}} \in \mathbb{F}_2^{l_{\mathcal{R}}^{\text{ENC}} + l_{\mathcal{R}}^{\text{KEY}}}$ ) and store the  $\lambda_{\mathcal{R}}^{\text{ENC}} + \lambda_{\mathcal{R}}^{\text{KEY}}$   $\blacksquare$  bits in  $V[\mathbf{c}_{\mathcal{R}}]$ .

195 Then, in each MitM episode, for a given  $\mathbf{c}_{\mathcal{B}}$  and  $\mathbf{c}_{\mathcal{R}}$ , the values in  $U[\mathbf{c}_{\mathcal{B}}]$  and  $V[\mathbf{c}_{\mathcal{R}}]$   
 196 can be searched in time  $O(1)$ . The time and memory cost for one precomputation  
 197 phase are both  $2^{\lambda_{\mathcal{B}}^{\text{ENC}} + \lambda_{\mathcal{B}}^{\text{KEY}}} + 2^{\lambda_{\mathcal{R}}^{\text{ENC}} + \lambda_{\mathcal{R}}^{\text{KEY}}}$ .

198 **SupP States and BiDir.** In the SupP MitM framework of [7], neutral cells  
 199 from both directions can be separated into two virtual states, called SupP states,  
 200 to keep the linearity through linear operations. Then,  $\blacksquare$  and  $\blacksquare$  will be treated  
 201 independently through linear operations, and the initial DoFs can be consumed  
 202 in both directions. After a series of linear operations, two SupP states are fi-  
 203 nally combined before the next nonlinear operation. The color patterns and how  
 204 the states are separated and combined are visualized in Figure 2. BiDir allows  
 205 neutral cells to be consumed in both two directions, but this may lead to depen-  
 206 dency between one type of neutral cell with non-linear constraints imposed on  
 207 another. In [11], Degré proposed a more generic table-based method to cancel  
 208 this dependency. Combined with the SupP states and BiDir methods, the solu-  
 209 tion space is greatly enlarged, such that some attack configurations with lower  
 210 time complexities may be found. In the rest of this paper, we simplify the repre-  
 211 sentation of SupP states. The virtual states of pure  $\blacksquare/\blacksquare/\blacksquare/\square$  are omitted. And  
 212 we denote the SupP states by the  $\blacksquare$  cell in which the blue cell and red cell occur  
 213 simultaneously.

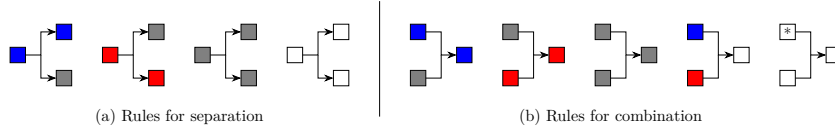


Fig. 2: Rules for separation and combination, where “\*” means any color

### 214 3 New Models for Linear Layer with Binary Matrix

215 In this section, we first propose an effective method to build an MILP model to  
 216 describe the MitM attributes propagation through a  $n$ -XOR operation with SupP  
 217 states. Interestingly, the number of input cells involved in the XOR operation  
 218 can be arbitrary, but the size of MILP model will not increase. However, we  
 219 also observe that this may lead to double counting of constraints on the same  
 220 neutral cells. Then, we show that the inaccuracy can be easily eliminated by  
 221 adding an additional check model.

#### 222 3.1 N-XOR Model

223 To simulate the MitM attributes propagation through the linear layer, Bao *et al.*  
 224 proposed the MC-RULE for the MDS matrix in AES-like hashing [6,7]. As shown  
 225 in Figure 3(a), each input cell has an effect on all output cells in MDS matrix.  
 226 However, some primitives adopt a binary matrix in the diffusion layer where  
 227 each output cell is computed by the XOR of partial input cells. As the Midori64’s  
 228 binary matrix shown in Figure 3(b), the first output cell is only related to the  
 229 last three input cells. Apparently, this will lead to inaccurate propagation if we  
 230 apply the MC-RULE for MDS matrix on binary matrix directly since one output  
 cell is not related to all input cells.



(a) Coloring pattern of MC-RULE for MDS matrix      (b) Coloring pattern for binary matrix

Fig. 3: A case of the difference of color pattern between MDS and binary matrix

231 In [13], Dong *et al.* proposed the 3-XOR-RULE to model the key addition in  
 232 SKINNY- $n-3n$ . By enumerating four input cells, one output cell and one indicator  
 233 variable for DoF cost, all valid color patterns can be restricted to a subset of  
 234  $\mathbb{F}_2^{11}$ , which can be described into a system of inequalities using the convex hull  
 235 technique [36]. If we directly extend the strategy of 3-XOR-RULE to the XOR  
 236 operation with  $n$  input cells, then the enumeration scope will be restricted to a  
 237

238 subset of  $\mathbb{F}_2^{2n+3}$ . When  $n$  is large, it's complicated and error-prone to enumerate  
 239 all valid color patterns. And the size of the system of inequalities may be large,  
 240 which renders the model infeasible to compute.

241 An alternative strategy is to apply the XOR-RULE in [6,7] for two-input XOR  
 242 consecutively. This strategy is valid but may miss some valid patterns by intro-  
 243 ducing additional auxiliary variables. We take the attribute propagation through  
 244 Midori64's diffusion layer to state this fact as shown in Figure 4. In the first step  
 245 of Figure 4(a), an auxiliary variable `auxi` is needed to carry on the output of  
 246  $X[2] \oplus X[3]$ . For the second step,  $X[1]$  and  $X[0]$  are XORed with `auxi` to compute  
 247  $Y[0]$  and  $Y[1]$ , respectively. Then, one of the following cases will occur,

- 248 – If `auxi` is ■ by consuming one DoF, then  $Y[0]$  will always be ■, and  $Y[1]$   
 249 will always be ■.
- 250 – If `auxi` is ■, then  $Y[1]$  will always be ■.  $Y[0]$  can be either ■ or ■ by consuming  
 251 one DoF.

252 However, with the n-XOR model in Figure 4(b), step 1 and step 2 can be exe-  
 253 cuted independently without correlated variables. Then,  $Y[0]$  and  $Y[1]$  can be  
 254 ■ simultaneously by consuming 2 DoFs of ■, which can not be captured by the  
 first strategy.

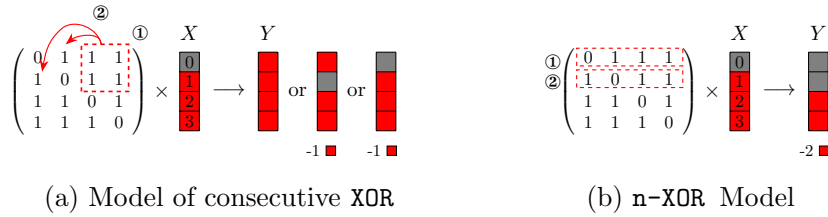


Fig. 4: The advantage of n-XOR model compared with consecutive XOR

255 In the following, we show how to convert the propagation of ■ cells through  
 256 the n-XOR operation under SupP states into MILP language. All coloring pat-  
 257 terns can be specified by the following set of rules denoted by n-XOR-RULE<sup>-</sup>.  
 258 The n-XOR-RULE<sup>+</sup> for ■ can be obtained in a similar way by exchanging ■ and  
 259 ■ since they are dual.

- 261 – n-XOR-RULE<sup>-</sup>-1. If there is at least one □ in input, then the output is □.
- 262 – n-XOR-RULE<sup>-</sup>-2. If all cells of the input are ■, then the output must be ■.
- 263 – n-XOR-RULE<sup>-</sup>-3. If there are ■ and ■ cells but no □ cell in the input, then  
 264 one of the following situations will occur:
  - 265 • The output is ■ cell and no DoF is consumed.
  - 266 • The output is ■ by consuming one DoF of ■.

267 Let  $(A[1], A[2], \dots, A[n])$  be the input of n-XOR where  $A[i] = (x_i^A, y_i^A)$ . Let  $B$  be  
 268 the output where  $B = (x^B, y^B)$ . Like [6], we introduce three boolean indicator



269 variables  $\mu, \nu$  and  $\eta$  in the model.  $\mu = 1$  if and only if there exists  $i \in [1, 2, \dots, n]$   
 270 such that  $(x_i^A, y_i^A) = (0, 0)$ . That is,  $\mathbf{n-XOR-RULE}^-1$  is fulfilled.  $\nu = 1$  if and only  
 271 if  $x_i^A = y_i^A = 1$  for all  $1 \leq i \leq n$ , which corresponds to  $\mathbf{n-XOR-RULE}^-2$ . When  
 272  $\mu = \nu = 0$ ,  $\mathbf{n-XOR-RULE}^-3$  is fulfilled. Besides,  $\eta = 1$  when there exists one  
 273 constraint imposed on input  $\blacksquare$  cells. With the help of indicator variables, the  
 274  $\mathbf{n-XOR-RULE}^-$  can be converted into a system of inequalities shown in Equation  
 (2) and Equation (3).

$$\begin{aligned}
 & \left\{ \begin{array}{l} \sum_{i=0}^{n-1} y_i^A + \mu \leq n \\ \sum_{i=0}^{n-1} y_i^A + n \cdot \mu \geq n \\ \sum_{i=0}^{n-1} x_i^A - \nu \leq n - 1 \\ \sum_{i=0}^{n-1} x_i^A - n \cdot \nu \geq 0 \end{array} \right. \quad (2) \quad \left\{ \begin{array}{l} y^B + \mu = 1 \\ x^B + \mu \leq 1 \\ \eta - x^B + \nu = 0 \\ \sum_{i=0}^{n-1} x_i^A + x^B - 2 \cdot \nu \leq n - 1 \\ \sum_{i=0}^{n-1} x_i^A + x^B - (n + 1) \cdot \nu \geq 0 \end{array} \right. \quad (3)
 \end{aligned}$$

275  
 276 At the end, we must emphasize that, in addition to preserving more valid  
 277 coloring patterns, another advantage of  $\mathbf{n-XOR}$  is that the size of model is fixed,  
 278 independent of the number of input cells. And this makes it possible to de-  
 279 scribe the attributes propagation for primitives with large binary matrices, like  
 280 *Camellia* and *Aria*.

### 281 3.2 Check Model: More Accurate Consumption of DoFs

282 We also observe that  $\mathbf{n-XOR}$  model may lead to some subtle inaccuracies. We still  
 283 take a possible propagation of *Midori64*'s diffusion layer as an example to state  
 284 this fact. A particularly explicit case is that the constraint on the same neutral  
 285 cells may be double counted due to the independent computation of each output  
 286 cell as shown in Figure 5(a). Besides, there are some more implicit cases leading  
 287 to inaccuracy as shown in Figure 5(b).

288 Then, we introduce the check model to show how the inaccuracy can be  
 289 eliminated, and describe it in the MILP language. We still state this by con-  
 290 sidering the  $\blacksquare$  propagation through the  $\mathbf{n-XOR}$  operation under SupP states. Let  
 291  $A[j] = (x_j^A, y_j^A)$ , for  $1 \leq j \leq n$ , be the input of the  $n \times n$  binary matrix  $M$ .  
 292 After the  $\mathbf{n-XOR}$  Model, we can get  $\boldsymbol{\eta} = (\eta_1, \dots, \eta_n)$  denoted by the degree con-  
 293 sumption vector where  $\eta_i$  is the indicator variable introduced in Equation (3)  
 294 and  $\eta_i = 1$  means there exists one constraint imposed on the input  $\blacksquare$  cells for the  
 295  $i$ -th row of  $M$ . Since only  $\blacksquare$  cells are needed to be considered for DoF consump-  
 296 tion, we introduce another  $n \times n$  binary matrix  $M'$  to intuitively mark which  $\blacksquare$   
 297 cells contribute to the DoF consumption. Then,  $M'$  is generated as follows :

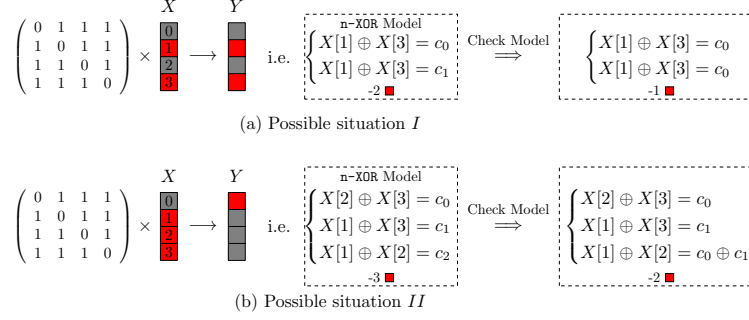


Fig. 5: Possible situations in our models

- 298 – If  $\eta_i = 1$  and  $M_{i,j} = 1$  and  $x_j^A = 0$ , then  $M'_{i,j} = 1$ .  
 299 – If the first case is not satisfied, then  $M'_{i,j} = 0$ .

300 For the first case,  $\eta_i = 1$  means no  $\square$  in the involved input cells, and  $M_{i,j} = 1$  and  
 301  $x_j^A = 0$  means  $A[j]$  is a  $\blacksquare$  cell involved in the  $i$ -th XOR operation. We introduce  
 302 a general variable  $\eta'$  to denote the rank of  $M'$ , which equals to the accurate  
 303 DoF consumption theoretically. Since  $M$  is a fixed matrix, we can conclude  
 304 that the accurate DoF consumption can be determined by the other  $2n$  vari-  
 305 ables  $(x_1^A, \dots, x_n^A, \eta_1, \dots, \eta_n)$ . Finally, the subset  $(x_1^A, \dots, x_n^A, \eta_1, \dots, \eta_n, \eta')$  of  
 306  $\mathbb{F}_2^{2n} \times \mathbb{F}_{n+1}$  can be restricted to a system of linear inequalities using the con-  
 307 vex hull technique [36]. Different with the origin framework, the configuration  
 308  $l_{\mathcal{R}}^{\text{ENC}} + l_{\mathcal{R}}^{\text{KEY}}$  should be calculated by accumulating the accurate DoF consumption  
 309 determined by the n-XOR and check model, along with extra constraints imposed  
 310 by other operations, such as **KeyAddition**. The configuration  $l_{\mathcal{B}}^{\text{ENC}} + l_{\mathcal{B}}^{\text{KEY}}$  for degree  
 311 consumption of  $\blacksquare$  can also be gotten in the similar way due to the duality [7].

312 However, it should be noted that the cost of exhaustion to determine the  
 313 accurate DoF consumption is still affected by the number of input cells. Hence,  
 314 check model can not be applied to large binary matrix ( $n > 4$  in this paper).  
 315 Although it's trivial to compute the rank of a general matrix in  $O(n^3)$ , there  
 316 is still no effective way to implement it in MILP model. Besides, in addition to  
 317 finding out better modeling methods or more suitable optimizers, we can still  
 318 combine theoretical models and manually checking to deal with large matri-  
 319 ces, such as Section 5 and Section 6. In practice, by relaxing the constraint to  
 320  $\min\{d_{\mathcal{B}}, d_{\mathcal{R}}, d_m\} \geq 1 - i$ , where  $i \geq 1$ , we check the feasible solutions to find out  
 321 valid characteristic. It also should be noted that the final results derived by the  
 322 manually checking method may not be the optimal solution.

## 323 4 MitM Key Recovery Attack on Midori64

324 Midori64 is an SPN-based lightweight block cipher, consisting of 64-bit block  
 325 and a 128-bit key. The state is seen as a  $4 \times 4$  matrix of 4-bit cells, and its

326 diffusion layer is  $4 \times 4$  boolean matrix. The detailed specification is provided in  
 327 Appendix B.1.

328 In this section, we present an 11-round MitM key recovery attack on Midori64  
 329 with a time complexity of  $2^{124}$ . For the weakened version of Midori64, without  
 330 whitening key, a 12-round MitM characteristic is found with a time complexity  
 331 of  $2^{120}$ . Despite a little higher time complexity, the above two attacks can be  
 332 applied with extremely low data and memory cost compared to the previous best  
 333 work [23,35]. Besides, the data and memory of the attack on 12-round weakened  
 334 Midori64 can be further reduced if the time complexity is relaxed to  $2^{124}$ .

#### 335 4.1 MitM Key Recovery Attack on 11-round Midori64

336 As shown in Figure 6 and Figure 7, an 11-round MitM key recovery attack is  
 337 identified, where  $|\mathcal{S}^{\text{ENC}}| = 16$  independent bytes in the encryption data path are  
 338 set to be 0 as Line 1-2 in Algorithm 1, to ensure the values of all the other bytes  
 339 are totally determined by the given key. And at least one 0 byte in the ciphertext  
 340  $C$  to avoid using the full codebook. The starting states are  $C$  and  $(K^{(0)}, K^{(1)})$ .  
 341 The encryption data path provides  $\lambda_{\mathcal{R}}^{\text{ENC}} = 9$  and  $\lambda_{\mathcal{B}}^{\text{ENC}} = 0$  DoFs for  $\blacksquare$  and  $\blacksquare$ ,  
 342 respectively. And the  $\lambda_{\mathcal{R}}^{\text{ENC}} = 9$   $\blacksquare$  cells are used up when computing  $A_{\text{Shc}}^{(9)}$  through  
 343 an MC operation and  $A_{\text{MC}}^{(8)}$  through an XOR operation in the backward computation  
 344 path. For  $(K^{(0)}, K^{(1)})$ , the initial DoFs for  $\blacksquare$  and  $\blacksquare$  are  $\lambda_{\mathcal{R}}^{\text{KEY}} = 3$  and  $\lambda_{\mathcal{B}}^{\text{KEY}} = 2$ ,  
 345 respectively. In the key schedule,  $K^{(0)}[1] \oplus K^{(0)}[9]$  and  $K^{(0)}[1] \oplus K^{(0)}[13]$  are  
 346 restricted to constants, i.e.,  $l_{\mathcal{R}}^{\text{KEY}} = 2$ . Hence, we get  $\text{DoF}_{\mathcal{R}} = \lambda_{\mathcal{R}}^{\text{KEY}} - l_{\mathcal{R}}^{\text{KEY}} = 1$ .  
 347 Similarly,  $K^{(0)}[5] \oplus K^{(1)}[5]$  is imposed on  $l_{\mathcal{B}}^{\text{KEY}} = 1$  constraint, and then  $\text{DoF}_{\mathcal{B}} =$   
 348  $\lambda_{\mathcal{B}}^{\text{KEY}} - l_{\mathcal{B}}^{\text{KEY}} = 1$ . The matching phase happens at the MC operation between  $A_{\text{Shc}}^{(3)}$   
 349 and  $A_{\text{MC}}^{(3)}$ , providing  $d_m = 1$  degree of matching by Equation (4).

$$A_{\text{Shc}}^{(3)}[2] \oplus A_{\text{Shc}}^{(3)}[10] = A_{\text{MC}}^{(3)}[2] \oplus A_{\text{MC}}^{(3)}[10] \quad (4)$$

350 According to Equation (1), the overall time complexity is  $2^{4 \times (32 - \min\{1,1,1\})} \approx$   
 351  $2^{124}$ . The data complexity is  $2^{36}$  by traversing the  $16 - 7 = 9$  non-constant cells  
 352 in  $C$ . A detailed attack procedure is given in Algorithm 1. The memory cost is  
 353 about  $2^6$  bytes to store  $(\mathcal{S}_{\mathcal{R}}, \mathcal{S}_{\mathcal{B}}, L)$ .

#### 354 4.2 MitM Key Recovery Attack on 12-round Weakened Midori64

355 In this section, we focus on the weakened version of Midori64 omitting the  
 356 whitening layers. And we found a MitM key recovery attack on the 12-round  
 357 Midori64 as shown in Figure 8. As explained above,  $|\mathcal{S}^{\text{ENC}}| = 16$  independent  $\blacksquare$   
 358 bytes in the encryption data path are set as 0. The starting states are ciphertext  
 359  $C$  and two sub-key  $(K^{(0)}, K^{(1)})$ . In ciphertext, there are  $\lambda_{\mathcal{R}}^{\text{ENC}} = 12$  and  $\lambda_{\mathcal{B}}^{\text{ENC}} = 0$   
 360 initial DoFs for  $\blacksquare$  and  $\blacksquare$ , respectively. And the DoFs of  $\blacksquare$  are used up when  
 361 computing  $A_{\text{Shc}}^{(10)}$  through an MC operation and  $A_{\text{MC}}^{(9)}$  through an XOR operation.  
 362 The two sub-key  $(K^{(0)}, K^{(1)})$  provide  $\lambda_{\mathcal{R}}^{\text{KEY}} = 6$  and  $\lambda_{\mathcal{B}}^{\text{KEY}} = 2$  initial DoFs for  $\blacksquare$   
 363 and  $\blacksquare$ , respectively. For the key schedule,  $K^{(0)}[0] \oplus K^{(0)}[4]$ ,  $K^{(0)}[0] \oplus K^{(0)}[8]$ ,

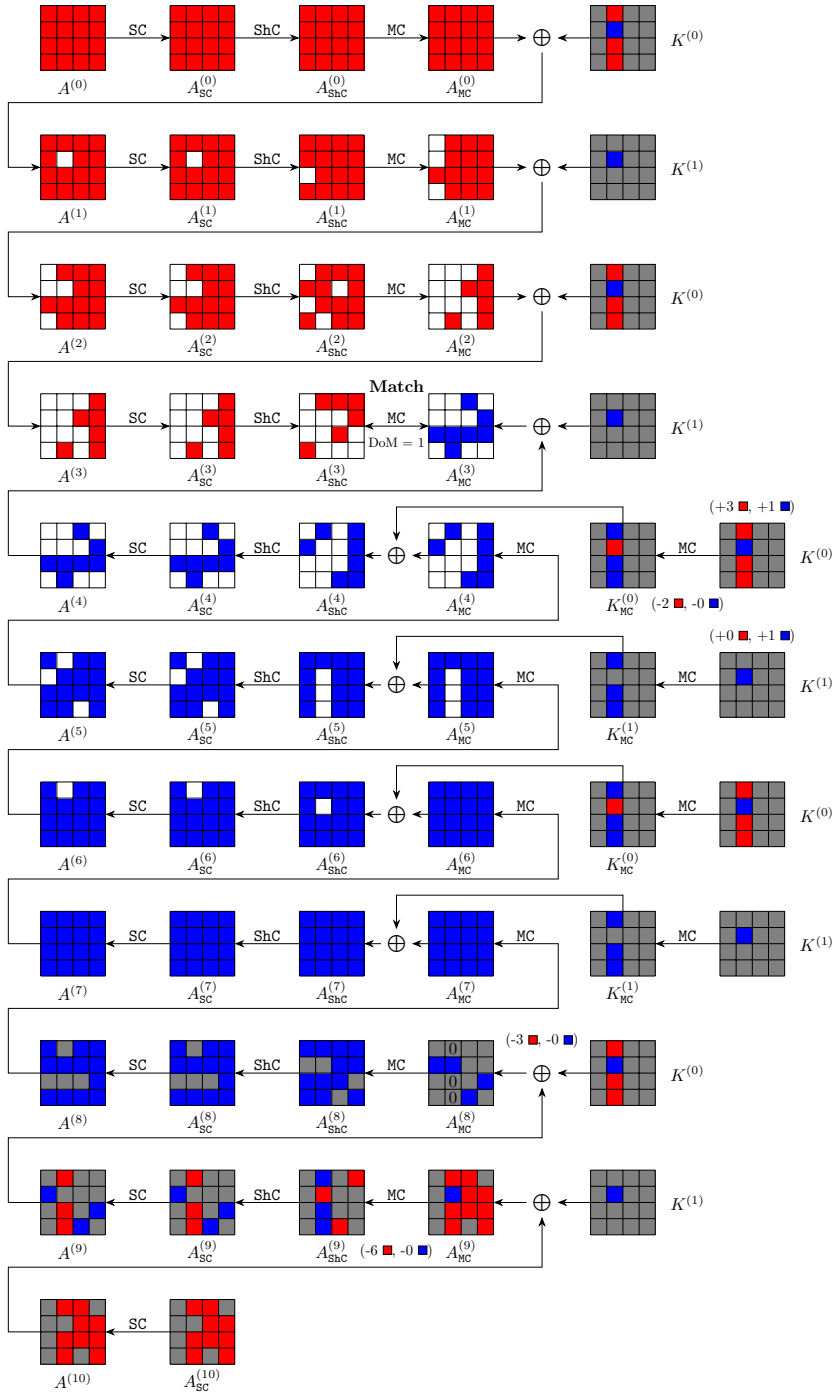


Fig. 6: Meet-in-the-Middle key recovery attack on 11-round Midori64

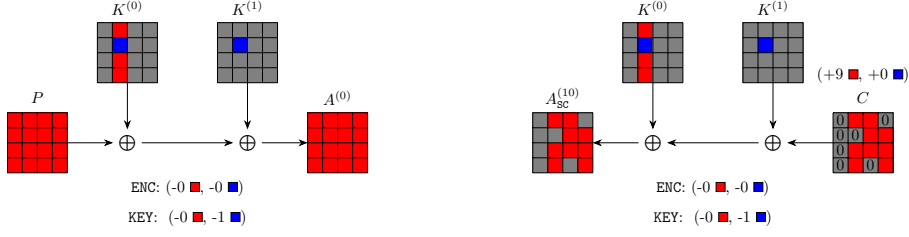


Fig. 7: The MitM characteristic through whitening layers of 11-round Midori64

---

**Algorithm 1: MitM Key Recovery Attack on 11-round Midori64**

---

```

1 Set the  $\blacksquare$  bytes to be 0, i.e.,  $C[0, 3, 4, 5, 8, 12, 14] \leftarrow 0$ ,  $A_{MC}^{(8)}[1, 9, 13] \leftarrow 0$ 
2  $A_{MC}^{(9)}[1] \oplus A_{MC}^{(9)}[9] \leftarrow 0$ ,  $A_{MC}^{(9)}[1] \oplus A_{MC}^{(9)}[13] \leftarrow 0$ ,  $A_{MC}^{(9)}[2] \oplus A_{MC}^{(9)}[6] \leftarrow 0$ ,
    $A_{MC}^{(9)}[2] \oplus A_{MC}^{(9)}[10] \leftarrow 0$ ,  $A_{MC}^{(9)}[7] \oplus A_{MC}^{(9)}[11] \leftarrow 0$ ,  $A_{MC}^{(9)}[7] \oplus A_{MC}^{(9)}[15] \leftarrow 0$ 
3 Collecting plaintext-ciphertext pairs by traversing the non-constant  $16 - 7 = 9$ 
   cells in  $C$ , and storing them in table  $H$ 
4 for all possible values of the  $\blacksquare$  cells in  $K^{(0)}$  and  $K^{(1)}$  do
5    $A_{SC}^{(10)}[0, 3, 4, 5, 8, 12, 14] \leftarrow (K^{(0)} \oplus K^{(1)})[0, 3, 4, 5, 8, 12, 14]$ 
6   for  $(c_{R,1}, c_{R,2}, c_B) \in \mathbb{F}_2^{3 \times 4}$  do
7     Derive the solution space  $\mathcal{S}_R$  of  $\blacksquare$  cells by
           
$$\begin{cases} K^{(0)}[1] \oplus K^{(0)}[9] = c_{R,1} \\ K^{(0)}[1] \oplus K^{(0)}[13] = c_{R,2} \end{cases}$$

8     Derive the solution space  $\mathcal{S}_B$  of  $\blacksquare$  cells by  $K^{(0)}[5] \oplus K^{(1)}[5] = c_B$ 
9      $L \leftarrow []$ 
10    for  $v_R \in \mathcal{S}_R$  do
11      Compute  $A_{ShC}^{(3)}[2, 10]$  along the forward computation path:
12       $A_{MC}^{(8)} \rightarrow C \rightarrow Dec_K(C) \rightarrow A_{ShC}^{(3)}$  by accessing  $H$ 
13       $L[A_{ShC}^{(3)}[2] \oplus A_{ShC}^{(3)}[10]] \leftarrow v_R$ 
14    end
15    for  $v_B \in \mathcal{S}_B$  do
16      Compute  $A_{MC}^{(3)}[2, 10]$  along the backward computation path:
            $C \rightarrow A_{MC}^{(3)}$ 
17      for Candidate keys in  $L[A_{MC}^{(3)}[2] \oplus A_{MC}^{(3)}[10]]$  do
18        | Test the guessed key with several plaintext-ciphertext pairs
19      end
20    end
21  end
22 end

```

---

364  $K^{(0)}[1] \oplus K^{(0)}[5]$  and  $K^{(0)}[1] \oplus K^{(0)}[13]$  are restricted to constants, i.e.,  $l_{\mathcal{R}}^{\text{KEY}} = 4$ .  
365 Hence, we get  $\text{DoF}_{\mathcal{R}} = \lambda_{\mathcal{R}}^{\text{KEY}} - l_{\mathcal{R}}^{\text{KEY}} = 2$  and  $\text{DoF}_{\mathcal{B}} = \lambda_{\mathcal{B}}^{\text{KEY}} = 2$ . The matching  
366 phase happens at the MC operation between  $A_{\text{ShC}}^{(4)}$  and  $A_{\text{MC}}^{(4)}$ , providing  $d_m = 1$   
367 degree of matching by Equation (5).

$$A_{\text{ShC}}^{(4)}[4] \oplus A_{\text{ShC}}^{(4)}[12] = A_{\text{MC}}^{(4)}[4] \oplus A_{\text{MC}}^{(4)}[12] \quad (5)$$

368 In [14], Fuhr *et al.* proposed the *simultaneous matching* to decrease  $2^{d_{\mathcal{B}}+d_{\mathcal{R}}-d_m}$  in  
369 Equation (1) exponentially by testing the surviving keys with multiple plaintext-  
370 ciphertext pairs in parallel. Hence, the overall time is dominated by  $2^{4 \times (32 - \min\{2,2\})} \approx$   
371  $2^{120}$ . The data complexity is  $2^{48}$  by traversing the  $16 - 4$  non-constant cells in  $C$ .  
372 A detailed attack procedure is given in Algorithm 2. The memory cost is  $2^{10.6}$   
373 bytes to store  $(\mathcal{S}_{\mathcal{R}}, L)$ .

374 When considering optimization for data complexity, we found a MitM key  
375 recovery attack on 12-round Midori64 with data complexity of  $2^{36}$  by relaxing  
376 the time complexity to  $2^{124}$ . The figure and algorithm are given in Figure 17  
377 and Algorithm 4 in Appendix C.

---

**Algorithm 2:** MitM Key Recovery Attack on 12-round weakened Midori64, optimized for time complexity

---

```

1  $C[2, 6, 10, 14] \leftarrow 0, A_{\text{ShC}}^{(10)}[1, 4, 7, 9, 12, 15] \leftarrow 0, A_{\text{MC}}^{(9)}[0, 1, 4, 5, 8, 13] \leftarrow 0$ 
2 Collecting plaintext-ciphertext pairs by traversing the non-constant
   16 - 4 = 12 cells in  $C$ , and storing them in table  $H$ 
3 for all possible values of the  $\blacksquare$  cells in  $K^{(0)}$  and  $K^{(1)}$  do
4   for  $(c_{\mathcal{R},1}, c_{\mathcal{R},2}, c_{\mathcal{R},3}, c_{\mathcal{R},4}) \in \mathbb{F}_2^{4 \times 4}$  do
5     Derive the solution space  $\mathcal{S}_{\mathcal{R}}$  of  $\blacksquare$  cells by
           
$$\begin{cases} K^{(0)}[0] \oplus K^{(0)}[4] = c_{\mathcal{R},1} & K^{(0)}[0] \oplus K^{(0)}[8] = c_{\mathcal{R},2} \\ K^{(0)}[1] \oplus K^{(0)}[5] = c_{\mathcal{R},3} & K^{(0)}[1] \oplus K^{(0)}[13] = c_{\mathcal{R},4} \end{cases}$$

6      $L \leftarrow []$ 
7     for  $v_{\mathcal{R}} \in \mathcal{S}_{\mathcal{R}}$  do
8       Compute  $A_{\text{ShC}}^{(4)}[4, 12]$  along the forward computation path:
9        $A_{\text{MC}}^{(9)} \rightarrow C \rightarrow \text{Dec}_K(C) \rightarrow A_{\text{ShC}}^{(4)}$  by accessing  $H$ 
10       $L[A_{\text{ShC}}^{(4)}[4] \oplus A_{\text{ShC}}^{(4)}[12]] \leftarrow v_{\mathcal{R}}$ 
11    end
12    for  $2^{2 \times 4}$  possible values of  $K^{(1)}[7, 12]$  do
13      Compute  $A_{\text{MC}}^{(4)}[4, 12]$  along the backward computation path:
           $C \rightarrow A_{\text{MC}}^{(4)}$ 
14      for Candidate keys in  $L[A_{\text{MC}}^{(4)}[4] \oplus A_{\text{MC}}^{(4)}[12]]$  do
15        | Test the guessed key with several plaintext-ciphertext pairs
16      end
17    end
18  end
19 end

```

---

## 378 5 MitM Preimage Attack on Weakened Camellia

379 Camellia is a Feistel-based block cipher with 128-bit block. The diffusion layer  
 380 is a  $8 \times 8$  boolean matrix. In this work, we only target on the version with a  
 381 128-bit key. The detailed specification is provided in Appendix B.2.

### 382 5.1 The MitM Characteristic of 14-round weakened Camellia

383 We first applied the n-XOR model to describe the attributes propagation through  
 384 the diffusion layer. However, the check model can not be deployed since the large  
 385 size of the diffusion layer. We relaxed the constraint to  $\min\{d_{\mathcal{B}}, d_{\mathcal{R}}, d_m\} \geq 1 - i$ ,  
 386 where  $i \geq 1$ , as stated in Section 3.2, and manually checked the solution files to  
 387 find out valid solutions (may not be optimal).

388 The final valid configuration of the pseudo-preimage MitM attack on 14-  
 389 round weakened Camellia-MMO without  $FL/FL^{-1}$  and whitening layers is shown  
 390 in Figure 9. We deploy the n-XOR model by considering the MixColumns and XOR  
 391 as a whole. The attack starts at  $A^{(9)}$  and  $B^{(9)}$  illustrated in Figure 9(a), in which  
 392 the initial DoFs for  $\blacksquare$  and  $\blacksquare$  are  $\lambda_{\mathcal{B}} = \lambda_{\mathcal{R}} = 7$ . In the forward computation path,  
 393 in order to facilitate the propagation of  $\blacksquare$  cells, there are  $l_{\mathcal{R}} = 6$  linear constraints  
 394 imposed on  $A_{\text{SB}}^{(9)}[7] \oplus B^{(9)}[i]$ , for  $i \in \{0, 1, 2, 4, 5, 6\}$ . Similarly, in the backward  
 395 computation path,  $l_{\mathcal{B}} = 6$  linear constraints are imposed on  $A_{\text{SB}}^{(8)}[7] \oplus A^{(9)}[i]$ ,  
 396 for  $i \in \{0, 1, 2, 4, 5, 6\}$ , to facilitate the propagation of  $\blacksquare$  cells. Hence, we get  
 397  $d_{\mathcal{B}} = \lambda_{\mathcal{B}} - l_{\mathcal{B}} = 1$  and  $d_{\mathcal{R}} = \lambda_{\mathcal{R}} - l_{\mathcal{R}} = 1$ .

398 Around the feed-forward mechanism of MMO mode, we set global constraints  
 399 on round keys  $(k_0, k_1, k_{12}, k_{13})$  to preserve some attributes like [28]. Specifically,  
 400 for the given target  $H_0 \| H_1$ ,  $A_{\text{SB}}^{(0)}$  equals to  $A_{\text{SB}}^{(13)}$  by setting  $k_0 = k_{13} \oplus H_0$  globally.  
 401 Since  $B^{(0)} = \text{MC}(A_{\text{SB}}^{(13)}) \oplus A^{(12)} \oplus H_1$  and  $A^{(1)} = B^{(0)} \oplus \text{MC}(A_{\text{SB}}^{(0)})$ , then we can get  
 402  $A^{(1)} = A^{(12)} \oplus H_1$ . Similarly,  $A^{(2)}$  equals to  $B^{(12)} \oplus H_0$  by setting  $k_1 = k_{12} \oplus H_1$ .  
 403 The cost to determine such proper subkeys is given in Section 5.2 and will not  
 404 exceed the time complexity of main MitM procedure.

405 The matching points are  $A^{(5)}$  and  $B^{(5)}$  in Figure 9(c). At first glance, there  
 406 are no degree for the direct matching. However, after applying a linear trans-  
 407 formation  $P^{-1}$  to  $B^{(5)}$  as in Figure 10, two-byte degree of match are derived.  
 408 Since  $d_{\mathcal{B}} = d_{\mathcal{R}} = 1$ , we only use one-byte for match, i.e.,  $d_m = 1$ . The specific  
 409 matching equation is Equation (6).

$$\bigoplus_{i \in \{0, 1, 2, 4, 5, 6\}} B^{(3)}[i] \oplus A_{\text{SB}}^{(3)}[3] = \bigoplus_{i \in \{0, 1, 2, 4, 5, 6\}} A^{(6)}[i] \oplus A_{\text{SB}}^{(5)}[3] \quad (6)$$

410 According to Equation (1), the total time complexity is bounded by  $2^{8 \times (16 - \min\{1, 1, 1\})} \approx$   
 411  $2^{120}$ . A detailed attack procedure is given in Algorithm 3. The memory complex-  
 412 ity of a hash table  $L$  is  $2^8$ . And this attack can be converted to a second preimage  
 413 attack with a time complexity of  $2^{125}$  according to [24, Fact9.99].

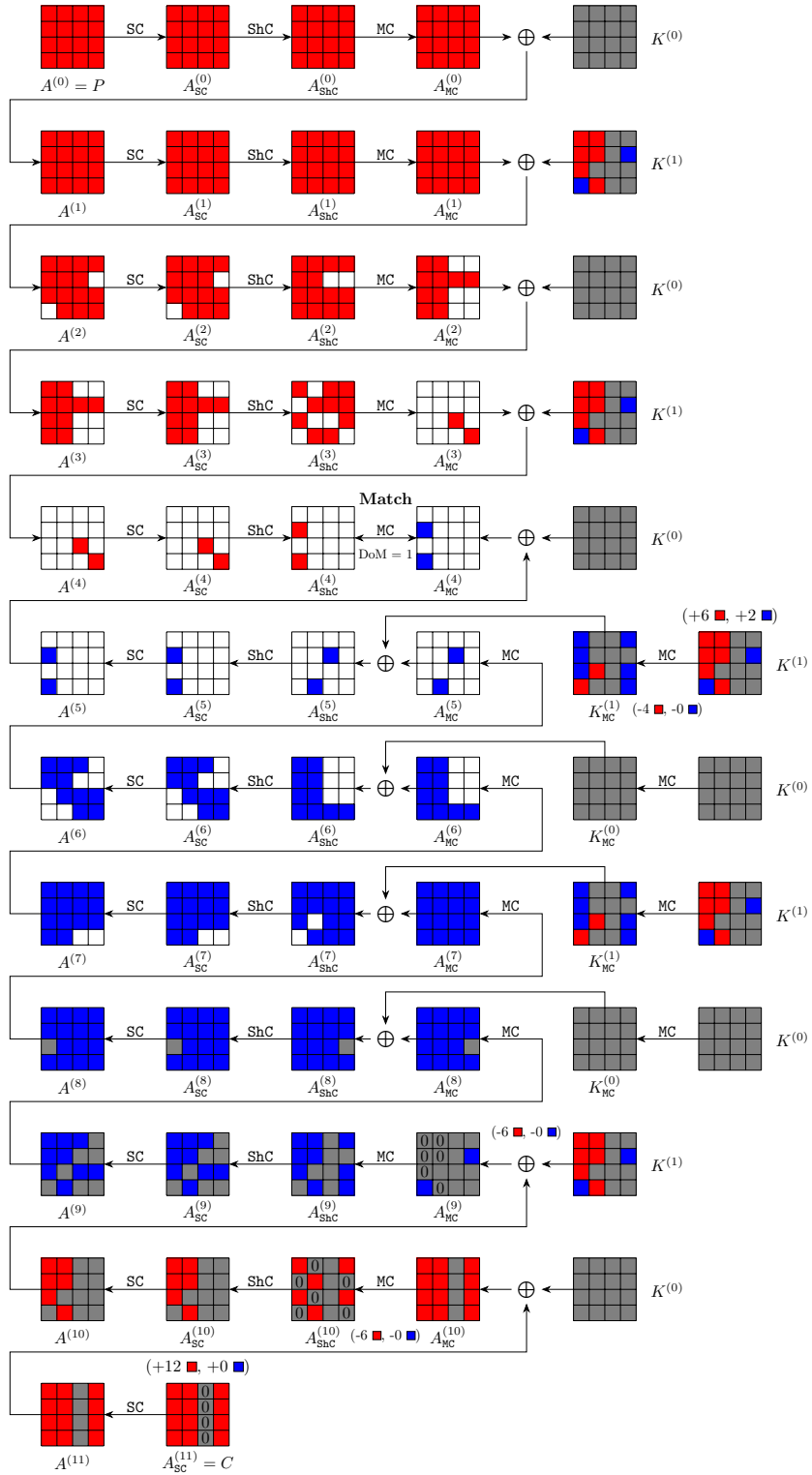


Fig. 8: Meet-in-the-Middle key recovery attack on 12-round weakened Midori64, optimized for time complexity



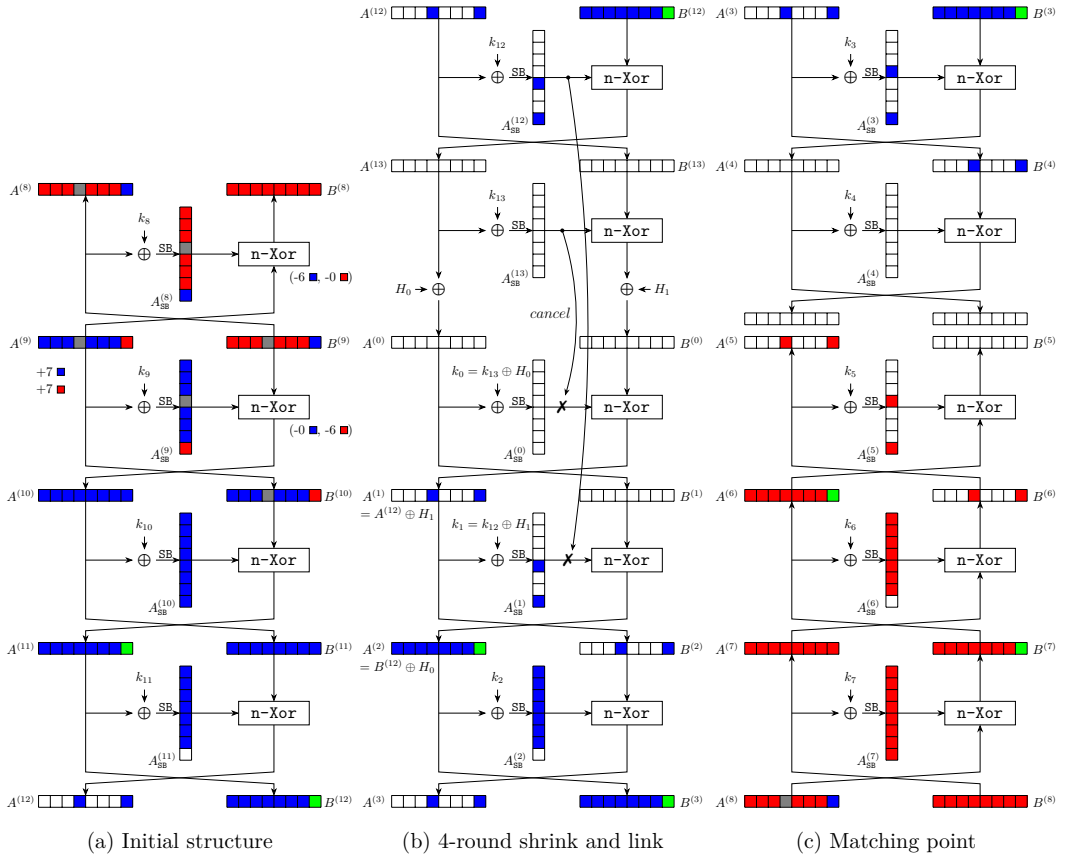


Fig.9: Meet-in-the-Middle pseudo-preimage attack on 14-round weakened Camellia-MMO

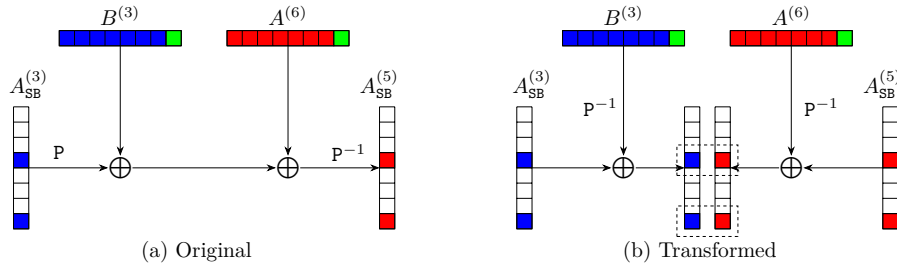


Fig.10: The matching process of 14-round weakened Camellia-MMO

---

**Algorithm 3:** MitM Pseudo-Preimage Attack on 14-round weakened Camellia-MMO

---

```

1 Setting a global key satisfying  $k_0 = k_{13} \oplus H_0$ ,  $k_1 = k_{12} \oplus H_1$ ;
2 for  $2^{16}$  values of the  $\blacksquare$  bytes in  $A^{(9)}[3]||B^{(9)}[3]$  do
3   for  $c_B \in \mathbb{F}_2^{8 \times 6}$  do
4     for  $c_R \in \mathbb{F}_2^{8 \times 6}$  do
5        $L \leftarrow []$ 
6       Solve the following system of equations to find the solution space
7          $\mathcal{S}_B$  of  $\blacksquare$  in  $A^{(9)}$  and  $B^{(9)}$ ; /*  $|\mathcal{S}_B| = 2^{8 \times (7-6)} = 2^8$  */

           $A_{SB}^{(8)}[7] \oplus A^{(9)}[0] = c_B[0]$ ,  $A_{SB}^{(8)}[7] \oplus A^{(9)}[1] = c_B[1]$ ,  $A_{SB}^{(8)}[7] \oplus A^{(9)}[2] = c_B[2]$ ,
           $A_{SB}^{(8)}[7] \oplus A^{(9)}[4] = c_B[3]$ ,  $A_{SB}^{(8)}[7] \oplus A^{(9)}[5] = c_B[4]$ ,  $A_{SB}^{(8)}[7] \oplus A^{(9)}[6] = c_B[5]$ .

8       Solve the following system of equations to find the solution space
9          $\mathcal{S}_R$  of  $\blacksquare$  in  $A^{(9)}$  and  $B^{(9)}$ ; /*  $|\mathcal{S}_B| = 2^{8 \times (7-6)} = 2^8$  */

           $A_{SB}^{(9)}[7] \oplus B^{(9)}[0] = c_R[0]$ ,  $B_{SB}^{(9)}[7] \oplus A^{(9)}[1] = c_R[1]$ ,  $A_{SB}^{(9)}[7] \oplus B^{(9)}[2] = c_R[2]$ ,
           $A_{SB}^{(9)}[7] \oplus B^{(9)}[4] = c_R[3]$ ,  $A_{SB}^{(9)}[7] \oplus B^{(9)}[5] = c_R[4]$ ,  $A_{SB}^{(9)}[7] \oplus B^{(9)}[6] = c_R[5]$ .

10      for  $v_B \in \mathcal{S}_B$  do
11        Compute forward to  $A^{(3)}$  and  $B^{(3)}$ , derive 1-byte  $End_B$  by
12           $End_B \leftarrow P^{-1}(B^{(3)})[3] \oplus A_{SB}^{(3)}[3]$ 
13           $L[End_B] \leftarrow v_B$ ;
14      end
15      for  $v_R \in \mathcal{S}_R$  do
16        Compute backward to  $A^{(6)}$  and  $B^{(6)}$ , derive 1-byte  $End_R$  by
17           $End_R \leftarrow P^{-1}(A^{(6)})[3] \oplus A_{SB}^{(5)}[3]$ 
18          for  $v_B \in L[End_R]$  do
19            Reconstruct the (candidate) message  $X$ ;
20            /*  $2^{8 \times (1+1-1)} = 2^8$  values passed the filter */
21            if  $X$  is a preimage then
22              Output  $X$  and stop;
23            end
24          end
25        end
26      end
27 end

```

---

414 **5.2 The Cost to Determine a Proper Key**

415 The key schedule of **Camellia** with 128-bit key is shown in Figure 15. As ex-  
 416 plained above, we only need to focus on  $(k_0, k_1, k_{12}, k_{13})$  [1],

$$k_0 \leftarrow K'_A, \quad k_1 \leftarrow K''_A, \quad k_{12} \leftarrow K''[30-63] \parallel K'[0-29], \quad k_{13} \leftarrow K'[30-63] \parallel K''[0-29].$$

417 As shown in Figure 15, every internal state can be derived for given  $K'$  and  
 418  $S_0$ . Hence, we get  $K'' = F_0(K') \oplus S_0$  and  $K''_A = F_2(F_1(S_0)) \oplus F_0(K')$ . According  
 419 to the global constraints  $k_0 = k_{13} \oplus H_0$  and  $k_1 = k_{12} \oplus H_1$ , the relation between  
 420  $K'$  and  $S_0$  can be represented as Equation (7).

$$F_2(F_1(S_0)) \oplus F_0(K') = (F_0(K') \oplus S_0)[30-63] \parallel K'[0-29] \oplus H_1 \quad (7)$$

421 Besides, we note that  $K'$  and  $S_0$  can be placed at two sides of Equation (8),  
 422 respectively. The left-hand-side of Equation (8) only contains variables in terms  
 423 of  $K'$ , while the right-hand-side of Equation (8) depends on  $S_0$ .

$$F_0(K') \oplus F_0(K')[30-63] \parallel K'[0-29] = F_2(F_1(S_0)) \oplus S_0[30-63] \parallel \overbrace{0 \cdots 0}^{30} \oplus H_1 \quad (8)$$

424 Then, an algebraic meet-in-the-middle attack can be mounted by enumerating  
 425  $K'$  and  $S_0$  independently to filter out valid pairs according to Equation (8), i.e.  
 426  $d_B = d_R = d_m = 64$ . The time and memory complexity are both  $2^{64}$ . Besides,  
 427 the memory cost can be further reduced by extracting partial  $x$  bits of  $K'$  and  
 428  $S_0$  as global variables. Then, the memory can be reduced by a fraction of  $2^x$ ,  
 429 while the total time is bounded by  $2^{64+x}$ . To avoid exceeding the time cost of  
 430 main MitM procedure,  $64 + x \leq 120$  should be fulfilled, i.e.,  $x$  can take 56 at  
 431 most. The corresponding memory cost is  $2^8$ .

432 **6 MitM Preimage Attack on 6-Round Aria**

433 **Aria** is an SPN-based block cipher that supports a 128-bit block. In this work,  
 434 we target on the version with a 128-bit key. The state is treated as a  $4 \times 4$  matrix.  
 435 And the diffusion layer is a  $16 \times 16$  boolean matrix. The detailed specification  
 436 of **Aria** is presented in Appendix B.3.

437 Since the large size diffusion layer, only the n-XOR model can be applied  
 438 to describe the MitM attribution propagation through the diffusion layer. By  
 439 relaxing the constraint to  $\min\{d_B, d_R, d_m\} \geq 1 - i$ , where  $i \geq 1$ , as stated in  
 440 Section 3.2, we finally found out a valid configuration of the pseudo-preimage  
 441 MitM attack on 6-round **Aria-DM** as shown in Figure 11 (may not be optimal).  
 442 The attack starts at  $A^{(1)}$  in which the initial DoFs for  $\blacksquare$  and  $\blacksquare$  are  $\lambda_B = 1$ ,  $\lambda_R =$   
 443 14, respectively. Since there are non-linear constraints on  $\blacksquare$  cells to compute  $A_{DL}^{(2)}$   
 444 through the DL operation. We use the table-based method in [13] to solve such  
 445 non-linear constraints.

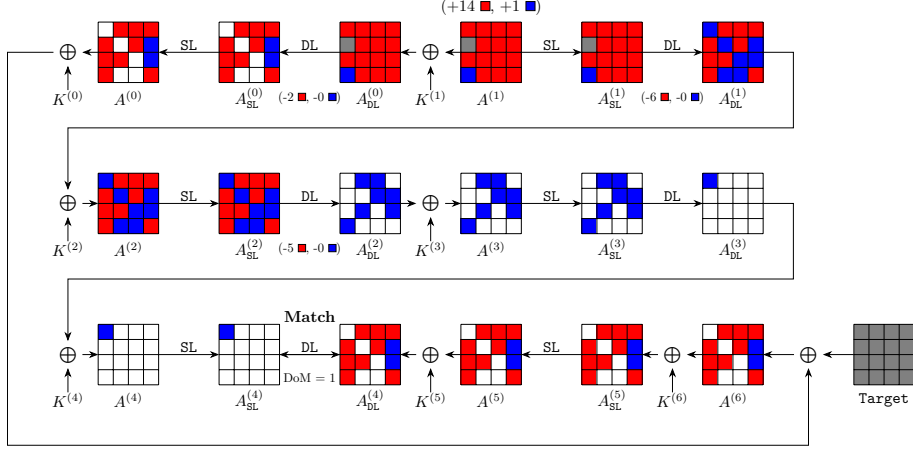


Fig. 11: Meet-in-the-Middle pseudo-preimage attack on 6-round Aria-DM

446 *Precomputation of red initial values.* By enumerating the ■ cells in  $A^{(1)}$ , in the  
 447 backward computation path, two constraints imposed on ■ cells can be computed  
 448 as follows:

$$\begin{cases} A_{DL}^{(0)}[0] \oplus A_{DL}^{(0)}[6] \oplus A_{DL}^{(0)}[7] \oplus A_{DL}^{(0)}[8] \oplus A_{DL}^{(0)}[10] \oplus A_{DL}^{(0)}[13] = c[0] \\ A_{DL}^{(0)}[0] \oplus A_{DL}^{(0)}[4] \oplus A_{DL}^{(0)}[5] \oplus A_{DL}^{(0)}[9] \oplus A_{DL}^{(0)}[11] \oplus A_{DL}^{(0)}[14] = c[1] \end{cases}$$

449 In the forward computation path, there are 11 constraints imposed on the ■  
 450 cells. During the DL operation in the 2nd round, 6 constraints are imposed on  
 451 the ■ cells. The specific expression of the constraints is shown in as follows:

$$\begin{cases} A_{SL}^{(1)}[4] \oplus A_{SL}^{(1)}[6] \oplus A_{SL}^{(1)}[8] \oplus A_{SL}^{(1)}[9] \oplus A_{SL}^{(1)}[13] \oplus A_{SL}^{(1)}[14] = c[2] \\ A_{SL}^{(1)}[4] \oplus A_{SL}^{(1)}[9] \oplus A_{SL}^{(1)}[10] \oplus A_{SL}^{(1)}[14] \oplus A_{SL}^{(1)}[15] = c[3] \\ A_{SL}^{(1)}[2] \oplus A_{SL}^{(1)}[5] \oplus A_{SL}^{(1)}[6] \oplus A_{SL}^{(1)}[8] \oplus A_{SL}^{(1)}[13] \oplus A_{SL}^{(1)}[15] = c[4] \\ A_{SL}^{(1)}[0] \oplus A_{SL}^{(1)}[6] \oplus A_{SL}^{(1)}[7] \oplus A_{SL}^{(1)}[8] \oplus A_{SL}^{(1)}[10] \oplus A_{SL}^{(1)}[13] = c[5] \\ A_{SL}^{(1)}[5] \oplus A_{SL}^{(1)}[7] \oplus A_{SL}^{(1)}[10] \oplus A_{SL}^{(1)}[11] = c[6] \\ A_{SL}^{(1)}[10] \oplus A_{SL}^{(1)}[11] \oplus A_{SL}^{(1)}[12] \oplus A_{SL}^{(1)}[15] = c[7] \end{cases}$$

452 Based on the above 6 constraints ( $c[2], c[3], c[4], c[5], c[6], c[7]$ ), the effect of the ■  
 453 cells on the 7 cells  $A_{DL}^{(1)}[0, 5, 7, 10, 11, 13, 14]$  can be cancelled as follows:

$$\begin{cases} A_{\text{SL}}^{(1)}[4] \oplus A_{\text{SL}}^{(1)}[6] \oplus A_{\text{SL}}^{(1)}[8] \oplus A_{\text{SL}}^{(1)}[9] \oplus A_{\text{SL}}^{(1)}[13] \oplus A_{\text{SL}}^{(1)}[14] = \mathbf{c}[2] \\ A_{\text{SL}}^{(1)}[4] \oplus A_{\text{SL}}^{(1)}[9] \oplus A_{\text{SL}}^{(1)}[10] \oplus A_{\text{SL}}^{(1)}[14] \oplus A_{\text{SL}}^{(1)}[15] = \mathbf{c}[3] \\ A_{\text{SL}}^{(1)}[6] \oplus A_{\text{SL}}^{(1)}[8] \oplus A_{\text{SL}}^{(1)}[11] \oplus A_{\text{SL}}^{(1)}[12] \oplus A_{\text{SL}}^{(1)}[13] = \mathbf{c}[2] \oplus \mathbf{c}[3] \oplus \mathbf{c}[7] \\ A_{\text{SL}}^{(1)}[2] \oplus A_{\text{SL}}^{(1)}[5] \oplus A_{\text{SL}}^{(1)}[6] \oplus A_{\text{SL}}^{(1)}[8] \oplus A_{\text{SL}}^{(1)}[13] \oplus A_{\text{SL}}^{(1)}[15] = \mathbf{c}[4] \\ A_{\text{SL}}^{(1)}[2] \oplus A_{\text{SL}}^{(1)}[4] \oplus A_{\text{SL}}^{(1)}[7] \oplus A_{\text{SL}}^{(1)}[9] \oplus A_{\text{SL}}^{(1)}[12] \oplus A_{\text{SL}}^{(1)}[14] = \mathbf{c}[2] \oplus \mathbf{c}[4] \oplus \mathbf{c}[6] \oplus \mathbf{c}[7] \\ A_{\text{SL}}^{(1)}[0] \oplus A_{\text{SL}}^{(1)}[6] \oplus A_{\text{SL}}^{(1)}[7] \oplus A_{\text{SL}}^{(1)}[8] \oplus A_{\text{SL}}^{(1)}[10] \oplus A_{\text{SL}}^{(1)}[13] = \mathbf{c}[5] \\ A_{\text{SL}}^{(1)}[0] \oplus A_{\text{SL}}^{(1)}[4] \oplus A_{\text{SL}}^{(1)}[5] \oplus A_{\text{SL}}^{(1)}[9] \oplus A_{\text{SL}}^{(1)}[11] \oplus A_{\text{SL}}^{(1)}[14] = \mathbf{c}[2] \oplus \mathbf{c}[5] \oplus \mathbf{c}[6] \end{cases}$$

454 In a similar way, the 5 constraints ( $\mathbf{c}[8], \mathbf{c}[9], \mathbf{c}[10], \mathbf{c}[11], \mathbf{c}[12]$ ) imposed on the  $\blacksquare$   
455 cells through the DL in the 3rd round are enough to cancel the effect of the  $\blacksquare$  cells  
456 on the 6 cells  $A_{\text{DL}}^{(2)}[4, 6, 8, 9, 13, 14]$ . For the specific expression of the constraints,  
457 please refer to Algorithm 5 in Appendix C. And the detailed DoFs consumption  
458 process is illustrated as follows:

$$\begin{cases} A_{\text{SL}}^{(2)}[2] \oplus A_{\text{SL}}^{(2)}[8] \oplus A_{\text{SL}}^{(2)}[15] = \mathbf{c}[8] \\ A_{\text{SL}}^{(2)}[2] \oplus A_{\text{SL}}^{(2)}[9] \oplus A_{\text{SL}}^{(2)}[12] = \mathbf{c}[8] \oplus \mathbf{c}[12] \\ A_{\text{SL}}^{(2)}[1] \oplus A_{\text{SL}}^{(2)}[4] \oplus A_{\text{SL}}^{(2)}[15] = \mathbf{c}[9] \\ A_{\text{SL}}^{(2)}[1] \oplus A_{\text{SL}}^{(2)}[6] \oplus A_{\text{SL}}^{(2)}[12] = \mathbf{c}[9] \oplus \mathbf{c}[11] \\ A_{\text{SL}}^{(2)}[3] \oplus A_{\text{SL}}^{(2)}[6] \oplus A_{\text{SL}}^{(2)}[8] = \mathbf{c}[10] \\ A_{\text{SL}}^{(2)}[3] \oplus A_{\text{SL}}^{(2)}[4] \oplus A_{\text{SL}}^{(2)}[9] = \mathbf{c}[10] \oplus \mathbf{c}[11] \oplus \mathbf{c}[12] \end{cases}$$

459 In summary, the values of  $l_{\mathcal{R}} = 13$  constraints can be determined for given values  
460 of  $\lambda_{\mathcal{R}} = 14$   $\blacksquare$  cells in  $A^{(1)}$ . Hence, we get  $d_{\mathcal{B}} = 1$ ,  $d_{\mathcal{R}} = \lambda_{\mathcal{R}} - l_{\mathcal{R}} = 1$ .

461 *Matching process.* The matching points are  $A_{\text{SL}}^{(4)}, A_{\text{DL}}^{(4)}$ , indirect matching through  
462 the DL provides one-byte match, i.e.,  $\text{DoM} = 1$ . The specific matching process is  
463 Equation (9).

$$A_{\text{SL}}^{(4)}[0] \oplus A_{\text{DL}}^{(4)}[13] \oplus A_{\text{DL}}^{(4)}[14] = A_{\text{DL}}^{(4)}[3] \oplus A_{\text{DL}}^{(4)}[4] \oplus A_{\text{DL}}^{(4)}[6] \oplus A_{\text{DL}}^{(4)}[8] \oplus A_{\text{DL}}^{(4)}[9] \quad (9)$$

464 Based on the above MitM framework, combined with the table-based tech-  
465 nique for solving nonlinear constrained neutral words [13], Algorithm 5 gives a  
466 detailed attack procedure in Appendix C.

467 *Complexity.* The nonlinear constraints imposed on  $\blacksquare$  cells are solved in Lines 2-8  
468 of Algorithm 5. That is, 14  $\blacksquare$  cells of  $A^{(1)}[0, 2, 4-15]$  are traversed to compute  
469 the exact values of  $\mathbf{c}_{\mathcal{R}}[0-12]$ . Then, the values of  $A^{(1)}[0, 2, 4-15]$  are stored in a  
470 hash table  $V$  under the index of  $\mathbf{c}_{\mathcal{R}}[0-12]$ . Hence, the time complexity of the  
471 precomputation phase is  $2^{8 \times 14} = 2^{112}$ . The memory complexity is also  $2^{112}$  to  
472 store table  $V$ .

473 Lines 10-24 of Algorithm 5 stand for one MitM episode. With the parameters  
474  $(d_{\mathcal{B}}, d_{\mathcal{R}}, d_m) = (1, 1, 1)$ , there are a total of  $2^{8 \times (1+1-1)} = 2^8$  solutions that can

475 be filtered out according to Equation (9). In order to find a full match of 128-  
 476 bit, it's expected to repeat  $2^{120-8} = 2^{112}$  MitM episodes. By traversing the  $\blacksquare$  in  
 477  $A^{(1)}$  at the outer loop and enumerating the 13 constraints imposed on  $\blacksquare$  cells,  
 478 it is sufficient to find a full match. According to Equation (1), The total time  
 479 complexity of the attack phase is

$$2^8 \times 2^{112} + 2^{8 \times (16 - \min\{1,1,1\})} \approx 2^{120}.$$

480 The memory complexity is dominated by the table  $V$  of  $2^{112}$ . And this attack  
 481 can be converted to a preimage attack with a time complexity of  $2^{125}$  according  
 482 to [24, Fact9.99].

## 483 7 Conclusion

484 In this paper, we propose the **n-XOR** model to simulate the XOR operation with  
 485 an arbitrary number of input cells. Specifically, the size of **n-XOR** model is inde-  
 486 pendent of the number of input cells, and thus it is well suitable for primitives  
 487 with a binary matrix as the diffusion layer. To eliminate the subtle inaccuracies  
 488 caused by **n-XOR** model, we introduce another check model to determine the ex-  
 489 act DoFs consumption of MitM attributes propagation. However, the size of the  
 490 check model is still limited by the number of input cells  $n$  and does not work well  
 491 when  $n > 4$  in this paper. We expect that there will be more elegant and efficient  
 492 techniques to overcome this defect and we leave this as an open problem.

493 We apply the above two new models to a MitM key recovery attack on 11-  
 494 round Midori64 with low data and memory. Besides, when omitting the whiten-  
 495 ing layers, two 12-round MitM characteristics for key recovery attack are found  
 496 for optimizing time and data, respectively. For hash functions, we obtain im-  
 497 proved preimage attack on 14-round weakened Camellia-MMO and 6-round Aria-  
 498 DM. Both attacks are improved by 1 round compared to previous best records.

## 499 References

- 500 1. Aoki, K., Ichikawa, T., Kanda, M., Matsui, M., Moriai, S., Nakajima, J., Tokita,  
 501 T.: Camellia: A 128-bit block cipher suitable for multiple platforms — design and-  
 502 analysis. In: Selected Areas in Cryptography. pp. 39–56. Springer Berlin Heidelberg  
 503 (2001). [https://doi.org/10.1007/3-540-44983-3\\_4](https://doi.org/10.1007/3-540-44983-3_4)
- 504 2. Aoki, K., Sasaki, Y.: Preimage attacks on one-block md4, 63-step md5 and more. In:  
 505 Selected Areas in Cryptography. pp. 103–119. Springer Berlin Heidelberg (2009).  
 506 [https://doi.org/10.1007/978-3-642-04159-4\\_7](https://doi.org/10.1007/978-3-642-04159-4_7)
- 507 3. Aumasson, J., Meier, W., Mendel, F.: Preimage attacks on 3-pass HAVAL and  
 508 step-reduced MD5. In: SAC. vol. 5381, pp. 120–135 (2008). [https://doi.org/10.](https://doi.org/10.1007/978-3-642-04159-4_8)  
 509 [1007/978-3-642-04159-4\\_8](https://doi.org/10.1007/978-3-642-04159-4_8)
- 510 4. Baek, S., Kim, J.: Quantum rebound attacks on reduced-round ARIA-based hash  
 511 functions. Cryptology ePrint Archive, Paper 2022/1604 (2022), [https://eprint.](https://eprint.iacr.org/2022/1604)  
 512 [iacr.org/2022/1604](https://eprint.iacr.org/2022/1604)

- 513 5. Banik, S., Bogdanov, A., Isobe, T., Shibutani, K., Hiwatari, H., Akishita,  
514 T., Regazzoni, F.: Midori: A block cipher for low energy. In: ASIACRYPT  
515 2015. pp. 411–436. Springer Berlin Heidelberg (2015). [https://doi.org/10.1007/](https://doi.org/10.1007/978-3-662-48800-3_17)  
516 [978-3-662-48800-3\\_17](https://doi.org/10.1007/978-3-662-48800-3_17)
- 517 6. Bao, Z., Dong, X., Guo, J., Li, Z., Shi, D., Sun, S., Wang, X.: Automatic search  
518 of meet-in-the-middle preimage attacks on aes-like hashing. In: EUROCRYPT  
519 2021. pp. 771–804. Springer International Publishing (2021). [https://doi.org/](https://doi.org/10.1007/978-3-030-77870-5_27)  
520 [10.1007/978-3-030-77870-5\\_27](https://doi.org/10.1007/978-3-030-77870-5_27)
- 521 7. Bao, Z., Guo, J., Shi, D., Tu, Y.: Superposition meet-in-the-middle attacks:  
522 updates on fundamental security of aes-like hashing. In: Annual International  
523 Cryptology Conference. pp. 64–93. Springer (2022). [https://doi.org/10.1007/](https://doi.org/10.1007/978-3-031-15802-5_3)  
524 [978-3-031-15802-5\\_3](https://doi.org/10.1007/978-3-031-15802-5_3)
- 525 8. Bogdanov, A., Khovratovich, D., Rechberger, C.: Biclique cryptanalysis of the full  
526 aes. In: Advances in Cryptology – ASIACRYPT 2011. pp. 344–371. Springer Berlin  
527 Heidelberg (2011). [https://doi.org/10.1007/978-3-642-25385-0\\_19](https://doi.org/10.1007/978-3-642-25385-0_19)
- 528 9. Bogdanov, A., Rechberger, C.: A 3-subset meet-in-the-middle attack: Cryptanalysis  
529 of the lightweight block cipher ktantan. In: SAC. pp. 229–240. Springer Berlin  
530 Heidelberg (2011). [https://doi.org/10.1007/978-3-642-19574-7\\_16](https://doi.org/10.1007/978-3-642-19574-7_16)
- 531 10. Chen, S., Guo, J., List, E., Shi, D., Zhang, T.: Diving deep into the preimage  
532 security of aes-like hashing. Cryptology ePrint Archive, Paper 2024/300 (2024),  
533 <https://eprint.iacr.org/2024/300>
- 534 11. Degré, M., Derbez, P., Lahaye, L., Schrottenloher, A.: New models for the crypt-  
535 analysis of ascon. Cryptology ePrint Archive, Paper 2024/298 (2024), [https:](https://eprint.iacr.org/2024/298)  
536 [//eprint.iacr.org/2024/298](https://eprint.iacr.org/2024/298)
- 537 12. Diffie, W., Hellman, M.E.: Special feature exhaustive cryptanalysis of the NBS  
538 data encryption standard. Computer **10**(6), 74–84 (1977). [https://doi.org/10.](https://doi.org/10.1109/C-M.1977.217750)  
539 [1109/C-M.1977.217750](https://doi.org/10.1109/C-M.1977.217750)
- 540 13. Dong, X., Hua, J., Sun, S., Li, Z., Wang, X., Hu, L.: Meet-in-the-middle attacks  
541 revisited: Key-recovery, collision, and preimage attacks. In: CRYPTO 2021. pp.  
542 278–308. Springer International Publishing (2021). [https://doi.org/10.1007/](https://doi.org/10.1007/978-3-030-84252-9_10)  
543 [978-3-030-84252-9\\_10](https://doi.org/10.1007/978-3-030-84252-9_10)
- 544 14. Fuhr, T., Minaud, B.: Match box meet-in-the-middle attack against KATAN. In:  
545 FSE 2014. pp. 61–81 (2014). [https://doi.org/10.1007/978-3-662-46706-0\\_4](https://doi.org/10.1007/978-3-662-46706-0_4)
- 546 15. Gurobi Optimization, LLC: Gurobi Optimizer Reference Manual (2023), [https:](https://www.gurobi.com)  
547 [//www.gurobi.com](https://www.gurobi.com)
- 548 16. Hong, D., Koo, B., Kim, D.C.: Preimage and second-preimage attacks on pgv  
549 hashing modes of round-reduced aria, camellia, and serpent. IEICE T Fund Electr  
550 **95**(1), 372–380 (2012), <https://api.semanticscholar.org/CorpusID:19830401>
- 551 17. Hou, Q., Dong, X., Qin, L., Zhang, G., Wang, X.: Automated meet-in-the-middle  
552 attack goes to feistel. In: ASIACRYPT 2023. pp. 370–404. Springer Nature Singa-  
553 pore (2023). [https://doi.org/10.1007/978-981-99-8727-6\\_13](https://doi.org/10.1007/978-981-99-8727-6_13)
- 554 18. Isobe, T.: A single-key attack on the full gost block cipher. Journal of cryptology  
555 **26**, 172–189 (2013). <https://doi.org/10.1007/s00145-012-9118-5>
- 556 19. ISO/IEC: 10118-2:2010 Information technology — Security techniques - Hash-  
557 functions - Part 2: Hash-functions using an n-bit block cipher, 3rd edn (2010)
- 558 20. ISO/IEC 18033-3:2010 Information technology-Security techniques-  
559 EncryptionAlgorithms-Part 3: Block ciphers (2010)
- 560 21. Kwon, D., Kim, J., Park, S., Sung, S.H., Sohn, Y., Song, J.H., Yeom, Y., Yoon,  
561 E.J., Lee, S., Lee, J., et al.: New block cipher: Aria. In: Inscrypt. pp. 432–445.  
562 Springer (2003). [https://doi.org/10.1007/978-3-540-24691-6\\_32](https://doi.org/10.1007/978-3-540-24691-6_32)

- 563 22. Lin, L., Wu, W.: Meet-in-the-middle attacks on reduced-round midori64. IACR  
564 ToSC pp. 215–239 (2017). <https://doi.org/10.13154/tosc.v2017.i1.215-239>
- 565 23. Liu, Y., Xiang, Z., Chen, S., Zhang, S., Zeng, X.: A novel automatic technique based  
566 on milp to search for impossible differentials. In: ACNS. pp. 119–148. Springer  
567 Nature Switzerland (2023). [https://doi.org/10.1007/978-3-031-33488-7\\_5](https://doi.org/10.1007/978-3-031-33488-7_5)
- 568 24. Menezes, A.J., Vanstone, S.A., Oorschot, P.C.V.: Handbook of Applied Cryptog-  
569 raphy. CRC Press, Inc., USA, 1st edn. (1996)
- 570 25. Preneel, B., Govaerts, R., Vandewalle, J.: Hash functions based on block ciphers:  
571 a synthetic approach. In: Advances in Cryptology — CRYPTO’ 93. pp. 368–378.  
572 Springer Berlin Heidelberg (1994). [https://doi.org/10.1007/3-540-48329-2\\_31](https://doi.org/10.1007/3-540-48329-2_31)
- 573 26. Sasaki, Y.: Meet-in-the-middle preimage attacks on aes hashing modes and an  
574 application to whirlpool. In: FSE. pp. 378–396. Springer Berlin Heidelberg (2011).  
575 [https://doi.org/10.1007/978-3-642-21702-9\\_22](https://doi.org/10.1007/978-3-642-21702-9_22)
- 576 27. Sasaki, Y.: Preimage attacks on feistel-sp functions: Impact of omitting the last  
577 network twist. In: ACNS. pp. 170–185. Springer Berlin Heidelberg (2013). [https://doi.org/10.1007/978-3-642-38980-1\\_11](https://doi.org/10.1007/978-3-642-38980-1_11)
- 578 28. Sasaki, Y.: Preimage attacks on feistel-sp functions: Impact of omitting the last  
579 network twist. IEICE T Fund Electr **98**(1), 61–71 (2015). <https://doi.org/10.1587/transfun.E98.A.61>
- 580 29. Sasaki, Y.: Integer linear programming for three-subset meet-in-the-middle attacks:  
581 Application to GIFT. In: IWSEC 2018. vol. 11049, pp. 227–243 (2018). [https://doi.org/10.1007/978-3-319-97916-8\\_15](https://doi.org/10.1007/978-3-319-97916-8_15)
- 582 30. Sasaki, Y., Aoki, K.: Finding preimages in full MD5 faster than exhaustive search.  
583 In: EUROCRYPT 2009, Proceedings. vol. 5479, pp. 134–152. Springer (2009).  
584 [https://doi.org/10.1007/978-3-642-01001-9\\_8](https://doi.org/10.1007/978-3-642-01001-9_8)
- 585 31. Sasaki, Y., Emami, S., Hong, D., Kumar, A.: Improved known-key distinguishers  
586 on feistel-sp ciphers and application to camellia. In: Information Security and Pri-  
587 vacy. pp. 87–100. Springer Berlin Heidelberg (2012). [https://doi.org/10.1007/978-3-642-31448-3\\_7](https://doi.org/10.1007/978-3-642-31448-3_7)
- 588 32. Sasaki, Y., Wang, L., Sakai, Y., Sakiyama, K., Ohta, K.: Three-subset meet-in-the-  
589 middle attack on reduced xtea. In: AFRICACRYPT 2012. pp. 138–154. Springer  
590 Berlin Heidelberg (2012). [https://doi.org/10.1007/978-3-642-31410-0\\_9](https://doi.org/10.1007/978-3-642-31410-0_9)
- 591 33. Schrottenloher, A., Stevens, M.: Simplified mitm modeling for permutations: New  
592 (quantum) attacks. In: CRYPTO 2022. pp. 717–747. Springer Nature Switzerland  
593 (2022). [https://doi.org/10.1007/978-3-031-15982-4\\_24](https://doi.org/10.1007/978-3-031-15982-4_24)
- 594 34. Schrottenloher, A., Stevens, M.: Simplified modeling of mitm attacks for block  
595 ciphers: New (quantum) attacks. IACR Transactions on Symmetric Cryptology  
596 **2023**, 146–183 (2023). <https://doi.org/10.46586/tosc.v2023.i3.146-183>
- 597 35. Shahmirzadi, A.R., Azimi, S.A., Salmasizadeh, M., Mohajeri, J., Aref, M.R.: Im-  
598 possible differential cryptanalysis of reduced-round midori64 block cipher. In: IS-  
599 CISC. pp. 99–104 (Sep 2017). <https://doi.org/10.1109/ISCISC.2017.8488362>
- 600 36. Sun, S., Hu, L., Wang, P., Qiao, K., Ma, X., Song, L.: Automatic security evalu-  
601 ation and (related-key) differential characteristic search: Application to SIMON,  
602 PRESENT, LBlock, DES(L) and other bit-oriented block ciphers. In: ASIACRYPT  
603 2014. pp. 158–178 (2014). [https://doi.org/10.1007/978-3-662-45611-8\\_9](https://doi.org/10.1007/978-3-662-45611-8_9)
- 604 37. Wei, L., Rechberger, C., Guo, J., Wu, H., Wang, H., Ling, S.: Improved meet-  
605 in-the-middle cryptanalysis of ktantan (poster). In: Information Security and Pri-  
606 vacy. pp. 433–438. Springer Berlin Heidelberg (2011). [https://doi.org/10.1007/978-3-642-22497-3\\_31](https://doi.org/10.1007/978-3-642-22497-3_31)
- 607  
608  
609  
610  
611



## 612 A Details of MILP Models for MitM Attack

613 In this section, we briefly recall the MILP model for MC and XOR operation of  
614 AES in [6].

615 **The MC.** The rules of the MC are formalized in two different directions in  
616 [6]. Taking the forward computation as an example, the set of rules is given as  
617 follows:

- 618 1. If there is at least one  $\square$  in the input column, all the outputs are  $\square$ ;
- 619 2. If there are  $\blacksquare$  but no  $\square$  and  $\blacksquare$  in the input column, then all the outputs are  
620  $\blacksquare$ ;
- 621 3. If all the inputs are  $\blacksquare$ , then all the outputs are  $\blacksquare$ ;
- 622 4. If there are  $\blacksquare$  and  $\blacksquare$  but no  $\square$  in the input column, each output must be  $\blacksquare$   
623 or  $\square$ . Moreover, the sum of the numbers of  $\blacksquare$  and  $\blacksquare$  in the input and output  
624 columns must be no more than 3;
- 625 5. If there are  $\blacksquare$  but no  $\square$  and  $\blacksquare$  in the input column, then each output must  
626 be  $\blacksquare$  or  $\blacksquare$ . Moreover, the number of  $\blacksquare$  in the input and output columns must  
627 be no more than 3.

628 Some examples of valid coloring schemes of the MC-RULE in the forward compu-  
629 tation are shown in Figure 12.

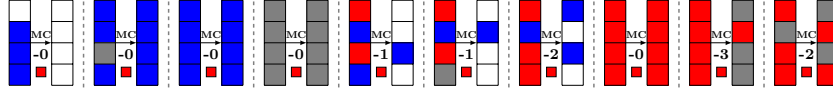


Fig. 12: Some valid coloring schemes for MC in forward computation in [6]

630 Let  $(\alpha[0], \alpha[1], \alpha[2], \alpha[3])^T$  and  $(\beta[0], \beta[1], \beta[2], \beta[3])^T$  be the input and output  
631 columns. In [6], Bao *et al.* use three 0-1 indicator variables  $\mu, v, \omega$  for the input  
632 column to fulfill different rules auxiliary. Let  $\mu = 1$  if and only if there exists  
633  $i \in \{0, 1, 2, 3\}$  such that  $(x_i^\alpha, y_i^\alpha) = (0, 0)$ . Let  $v = 1$  if and only if  $x_i^\alpha = 1$  for  
634 each  $i \in \{0, 1, 2, 3\}$ . Let  $\omega = 1$  if and only if  $y_i^\alpha = 1$  for each  $i \in \{0, 1, 2, 3\}$ .  
635 Then, with the help of  $\mu, v, \omega$ , the MC-RULE in the forward computation can be  
636 described as a system of inequalities:

$$\left\{ \begin{array}{l} \sum_{i=0}^3 x_i^\alpha - 4v \geq 0; \\ \sum_{i=0}^3 x_i^\alpha - v \leq 3. \end{array} \right. \left| \left\{ \begin{array}{l} \sum_{i=0}^3 x_i^\beta + 4\mu \leq 4; \\ \sum_{i=0}^3 y_i^\beta + 4\mu \leq 4; \\ \sum_{i=0}^3 y_i^\beta - 4\omega = 0; \end{array} \right. \right. \left\{ \begin{array}{l} \sum_{i=0}^3 (x_i^\alpha + x_i^\beta) - 5v \leq 3; \\ \sum_{i=0}^3 (x_i^\alpha + x_i^\beta) - 8v \geq 0. \end{array} \right.$$

637 **The XOR.** For the XOR operation in two different directions, the coloring  
 638 schemes of the input and output cells are shown in Figure 13.

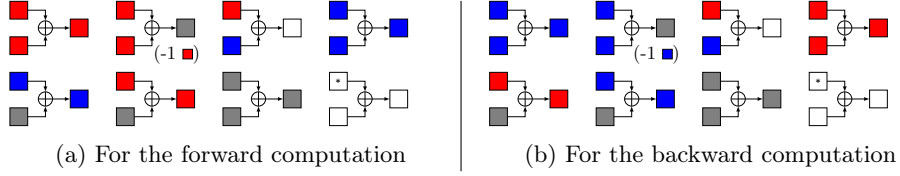


Fig. 13: The XOR in [6], where a “\*” means that the cell can be any color

638 Let  $\alpha[i]$ ,  $\beta[i]$  denote the input cells and  $\gamma[i]$  denote the output cell, where  
 639  $0 \leq i \leq 15$ . Let a boolean variable  $d_i$  indicate the consumption of DoF, where  
 640  $d_i = 1$  means that one DoF is consumed to let the corresponding output be  $\blacksquare$ .  
 641 The set of rules restrict  $(x_i^\alpha, y_i^\alpha, x_i^\beta, y_i^\beta, x_i^\gamma, y_i^\gamma, d_i)$  to a subset of  $\mathbb{F}_2^7$ , which can  
 642 be described by a system of linear inequalities with the convex hull technique in  
 643 [36].  
 644

## 645 B Descriptions of Midori, Camellia and Aria

### 646 B.1 Specification of Midori

647 Midori is a family of SPN-based lightweight block cipher designed by Banik *et*  
 648 *al.* at ASIACRYPT 2015 [5]. With its low energy consumption, it is suitable for  
 649 deployment in edge gateways and end devices to facilitate blockchain on-chain  
 650 and off-chain interactions. Two versions of Midori use a 64-bit and a 128-bit  
 651 internal state, respectively. In this work, we focus on the 64-bit version denoted  
 652 by Midori64. The internal state of Midori64 can be represented as a  $4 \times 4$  array  
 653 as shown in Figure 14. Midori64 is of 16 iterated rounds and each round function  
 654 consists of four operations:

- 655 - SubCell (SC): Apply the 4-bit non-linear involution S-box on each nibble.
- 656 - ShuffleCell (ShC): Update the position of each nibble by a pre-defined  
 657 permutation.
- 658 - MixColumn (MC): Each column is left multiplied by a  $4 \times 4$  binary matrix  
 659  $M$  as follows.

$$M = \begin{pmatrix} 0 & 1 & 1 & 1 \\ 1 & 0 & 1 & 1 \\ 1 & 1 & 0 & 1 \\ 1 & 1 & 1 & 0 \end{pmatrix}.$$

- 660 - KeyAdd (KA): A round key is XORed to the internal state.

661 For the last round, the operations ShC, MC and KA are omitted. Two sub-keys  
 662  $K^{(0)} \| K^{(1)}$  are derived from the 128-bit master key  $K$  and the round keys are

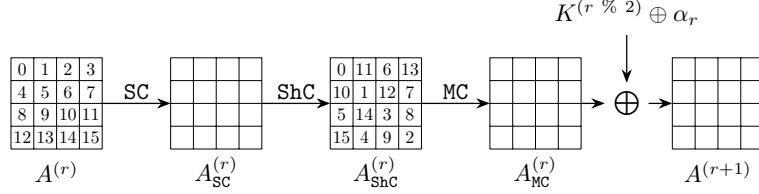


Fig. 14: One full round function of Midori64

663 generated by  $K^{(r \% 2)} \oplus \alpha_r$  alternatively, where  $0 \leq r \leq 14$  and  $\alpha_r$  is a round  
 664 constant. Besides, additional KA operations are applied with a whitening key  
 665  $WK = K^{(0)} \oplus K^{(1)}$  before the first round and after the last round.

## 666 B.2 Specification of Camellia

667 **Camellia** is a Feistel-based block cipher designed by NTT and Mitsubishi Elec-  
 668 tric Corporation [1] and has been specified in ISO/IEC 18033-3:2010 [20]. This  
 669 work only targets on the weakened version of **Camellia** with 128 bits block and  
 670 key size, where the  $FL/FL^{-1}$  transformations and whitening layers are omitted.  
 671 The iterated round function consists of **AddRoundKey** (AK), **SubBytes** (SB) and  
 672 **MixColumns** (MC) as shown in Figure 15. The linear layer of MC is a  $8 \times 8$  binary  
 673 matrix described as follows.

$$P = \begin{pmatrix} 1 & 0 & 1 & 1 & 0 & 1 & 1 & 1 \\ 1 & 1 & 0 & 1 & 1 & 0 & 1 & 1 \\ 1 & 1 & 1 & 0 & 1 & 1 & 0 & 1 \\ 0 & 1 & 1 & 1 & 1 & 1 & 1 & 0 \\ 1 & 1 & 0 & 0 & 0 & 1 & 1 & 1 \\ 0 & 1 & 1 & 0 & 1 & 0 & 1 & 1 \\ 0 & 0 & 1 & 1 & 1 & 1 & 0 & 1 \\ 1 & 0 & 0 & 1 & 1 & 1 & 1 & 0 \end{pmatrix}.$$

674 The key schedule takes a 128-bit key  $K = K' \| K''$  as the input of 4-round Feistel  
 675 structure, as shown in Figure 15, to compute another 128-bit key  $K_A = K'_A \| K''_A$ .  
 676 The round function is borrowed from the encryption, where the round keys  
 677 are pre-defined constants. Then, each round key  $k_i$  can be derived from the  
 678 rotation of  $K$  or  $K_A$ . Since we only focus on  $(k_0, k_1, k_{12}, k_{13})$ , we omit detailed  
 679 key schedule here.

## 680 B.3 Specification of Aria

681 **Aria** was proposed by Korean researchers at ICISC 2003 [21] and the version  
 682 1.2 was subsequently included in the Korean Standard (KS X1213) in 2004. In  
 683 this paper, we focus our attention on **Aria-128**, which refers to both the block  
 684 and key sizes are 128 bits, and which we henceforth abbreviate as **Aria**. **Aria**

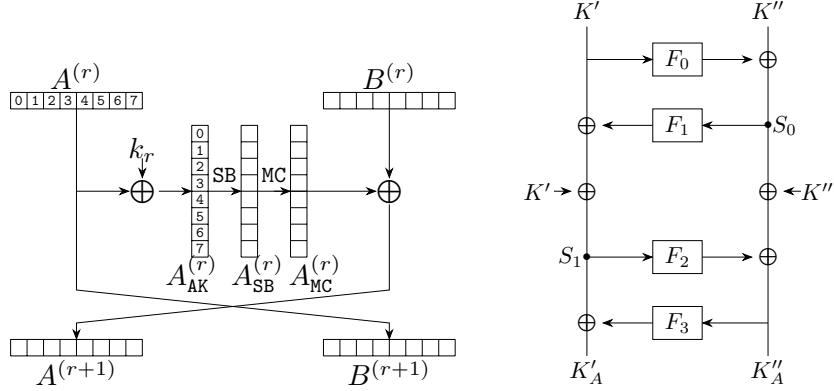


Fig. 15: One full round function of Camellia and the key schedule of Camellia

685 is based on SPN structure with 12 rounds, and each round except the last one  
 686 consists of Substitution-Layer (SL), Diffusion-Layer (DL) and AddRoundKey  
 687 (AK) as shown in Figure 16. In the last round, the DL is omitted. Before the first  
 688 round, a whitening key is XORed to the plaintext. The updated matrix  $P$  used in  
 689 DL is a  $16 \times 16$  binary matrix described as follows.

$$P = \begin{pmatrix} 0 & 0 & 0 & 1 & 1 & 0 & 1 & 0 & 1 & 1 & 1 & 0 & 0 & 0 & 1 & 1 & 0 \\ 0 & 0 & 1 & 0 & 0 & 1 & 0 & 1 & 1 & 1 & 1 & 0 & 0 & 1 & 0 & 0 & 1 \\ 0 & 1 & 0 & 0 & 1 & 0 & 1 & 0 & 0 & 0 & 1 & 1 & 1 & 1 & 0 & 0 & 1 \\ 1 & 0 & 0 & 0 & 0 & 1 & 0 & 1 & 0 & 0 & 1 & 1 & 1 & 0 & 1 & 1 & 0 \\ 1 & 0 & 1 & 0 & 0 & 1 & 0 & 0 & 1 & 0 & 0 & 1 & 0 & 0 & 1 & 1 & 1 \\ 0 & 1 & 0 & 1 & 1 & 0 & 0 & 0 & 0 & 1 & 1 & 0 & 0 & 0 & 1 & 1 & 1 \\ 1 & 0 & 1 & 0 & 0 & 0 & 0 & 1 & 0 & 1 & 1 & 0 & 1 & 1 & 0 & 0 & 0 \\ 0 & 1 & 0 & 1 & 0 & 0 & 1 & 0 & 1 & 0 & 0 & 1 & 1 & 1 & 1 & 0 & 0 \\ 1 & 1 & 0 & 0 & 1 & 0 & 0 & 1 & 0 & 0 & 1 & 0 & 0 & 1 & 0 & 1 & 0 \\ 1 & 1 & 0 & 0 & 0 & 1 & 1 & 0 & 0 & 0 & 0 & 1 & 1 & 0 & 1 & 0 & 1 \\ 0 & 0 & 1 & 1 & 0 & 1 & 1 & 0 & 1 & 0 & 0 & 0 & 0 & 1 & 0 & 1 & 0 \\ 0 & 0 & 1 & 1 & 1 & 0 & 0 & 1 & 0 & 1 & 0 & 0 & 1 & 0 & 1 & 0 & 1 \\ 0 & 1 & 1 & 0 & 0 & 0 & 1 & 1 & 0 & 1 & 0 & 1 & 1 & 0 & 0 & 0 & 0 \\ 1 & 0 & 0 & 1 & 0 & 0 & 1 & 1 & 1 & 0 & 1 & 0 & 0 & 1 & 0 & 0 & 0 \\ 1 & 0 & 0 & 1 & 1 & 1 & 0 & 0 & 0 & 1 & 0 & 1 & 0 & 0 & 1 & 0 & 1 \\ 0 & 1 & 1 & 0 & 1 & 1 & 0 & 0 & 1 & 0 & 1 & 0 & 0 & 0 & 0 & 1 & 1 \end{pmatrix}.$$

690 In this paper, we target on the preimage attack on Aria-DM. Since the key is  
 691 usually fixed as a constant in the DM hashing mode, we omit the description of  
 692 the key schedule here.

## 693 C Figure and algorithms for Midori64 and Aria

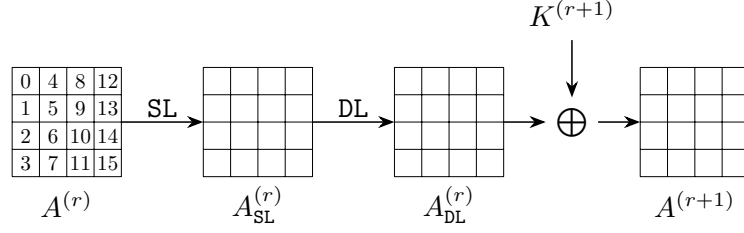


Fig. 16: One full round function of **Aria**

---

**Algorithm 4:** MitM Key Recovery Attack on 12-round weakened Midori64, , optimized for data complexity

---

```

1  $C[1, 3, 5, 8, 9, 13, 14] \leftarrow 0, A_{\text{MC}}^{(9)}[5, 9, 13] \leftarrow 0$ 
2  $A_{\text{MC}}^{(10)}[0] \oplus A_{\text{MC}}^{(10)}[4] \leftarrow 0, A_{\text{MC}}^{(10)}[0] \oplus A_{\text{MC}}^{(10)}[12] \leftarrow 0, A_{\text{MC}}^{(10)}[2] \oplus A_{\text{MC}}^{(10)}[6] \leftarrow 0,$ 
    $A_{\text{MC}}^{(10)}[2] \oplus A_{\text{MC}}^{(10)}[10] \leftarrow 0, A_{\text{MC}}^{(10)}[7] \oplus A_{\text{MC}}^{(10)}[11] \leftarrow 0, A_{\text{MC}}^{(10)}[7] \oplus A_{\text{MC}}^{(10)}[15] \leftarrow 0$ 
3 Collecting plaintext-ciphertext pairs by traversing the non-constant  $16 - 7 = 9$ 
   cells in  $C$ , and storing them in table  $H$ 
4 for all possible values of the  $\blacksquare$  cells in  $K^{(0)}$  and  $K^{(1)}$  do
5   for  $(c_{\mathcal{R},1}, c_{\mathcal{R},2}) \in \mathbb{F}_2^{2 \times 4}$  do
6     Derive the solution space  $\mathcal{S}_{\mathcal{R}}$  of  $\blacksquare$  cells by
           
$$\begin{cases} K^{(0)}[5] \oplus K^{(0)}[9] = c_{\mathcal{R},1} \\ K^{(0)}[5] \oplus K^{(0)}[13] = c_{\mathcal{R},2} \end{cases}$$

7      $L \leftarrow []$ 
8     for  $v_{\mathcal{R}} \in \mathcal{S}_{\mathcal{R}}$  do
9       Compute  $A_{\text{ShC}}^{(4)}[0, 4]$  along the forward computation path:
10       $A_{\text{MC}}^{(9)} \rightarrow C \rightarrow \text{Dec}_K(C) \rightarrow A_{\text{ShC}}^{(4)}$  by accessing  $H$ 
11       $L[A_{\text{ShC}}^{(4)}[0] \oplus A_{\text{ShC}}^{(4)}[4]] \leftarrow v_{\mathcal{R}}$ 
12    end
13    for  $2^4$  possible values of  $K^{(1)}[15]$  do
14      Compute  $A_{\text{MC}}^{(4)}[0, 4]$  along the backward computation path:
15       $C \rightarrow A_{\text{MC}}^{(4)}$ 
16      for Candidate keys in  $L[A_{\text{MC}}^{(4)}[0] \oplus A_{\text{MC}}^{(4)}[4]]$  do
17        Test the guessed key with several plaintext-ciphertext pairs
18      end
19    end
20 end

```

---

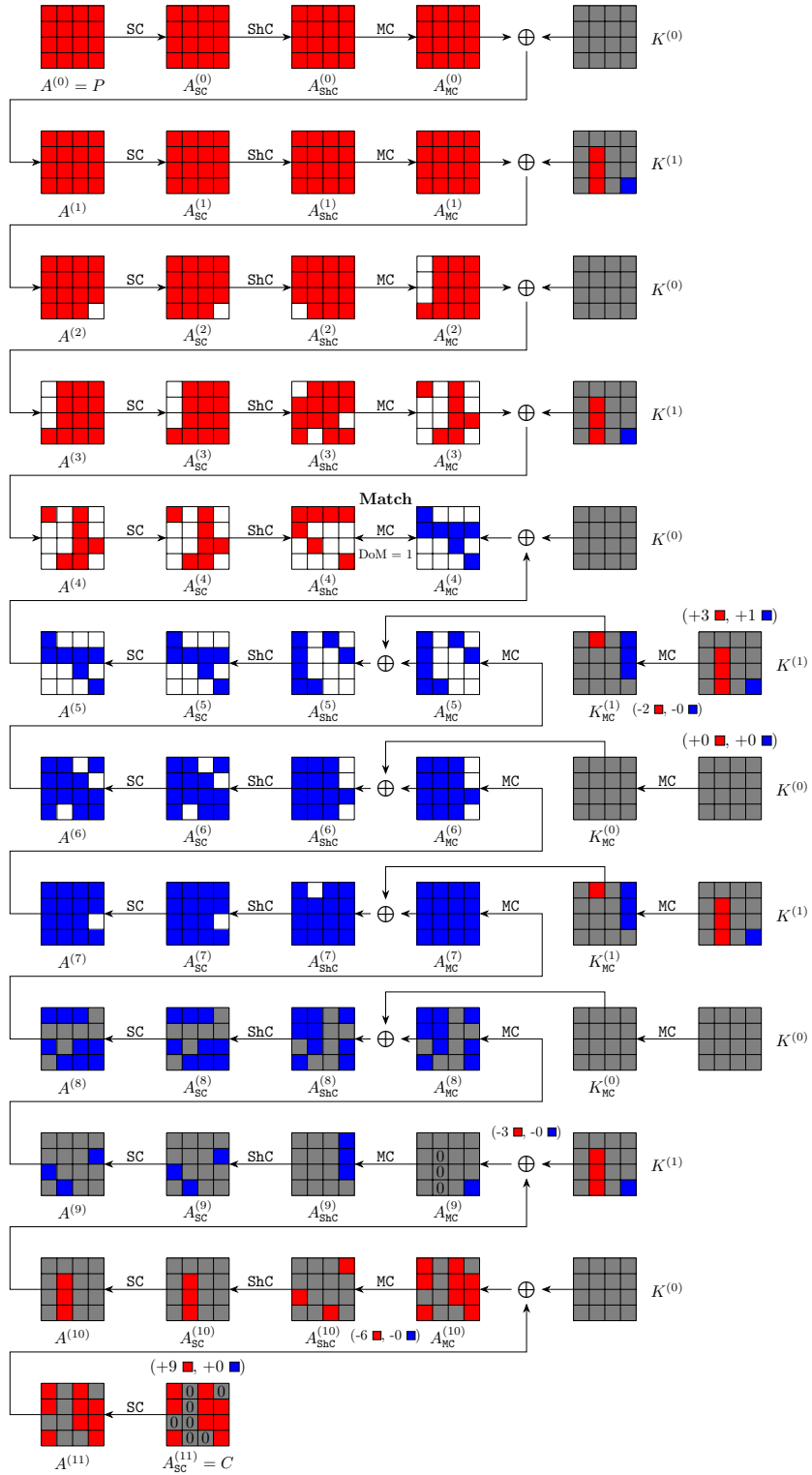


Fig.17: Meet-in-the-Middle key recovery attack on 12-round weakened Midori64, optimized for data complexity

---

**Algorithm 5: MitM Pseudo-Preimage Attack on 6-round Aria-DM**

---

```
1 for  $2^x$  possible values of  $\blacksquare$  in  $A^{(1)}$  /*  $x + 104 = 120 - 8$ , i.e.,  $x = 8$  */
2 do
3    $V \leftarrow []$ ;
4   for  $v_{\mathcal{R}} \in \mathbb{F}_2^{8 \times 14}$  in  $A^{(1)}$  do
5     Compute backward to get the values of the  $\blacksquare$  cells in  $A_{\text{DL}}^{(0)}$ ,
        
$$c_{\mathcal{R}}[0] \leftarrow A_{\text{DL}}^{(0)}[0] \oplus A_{\text{DL}}^{(0)}[6] \oplus A_{\text{DL}}^{(0)}[7] \oplus A_{\text{DL}}^{(0)}[8] \oplus A_{\text{DL}}^{(0)}[10] \oplus A_{\text{DL}}^{(0)}[13],$$

        
$$c_{\mathcal{R}}[1] \leftarrow A_{\text{DL}}^{(0)}[0] \oplus A_{\text{DL}}^{(0)}[4] \oplus A_{\text{DL}}^{(0)}[5] \oplus A_{\text{DL}}^{(0)}[9] \oplus A_{\text{DL}}^{(0)}[11] \oplus A_{\text{DL}}^{(0)}[14].$$

6     Compute forward to the  $\blacksquare$  cells in  $A_{\text{SL}}^{(1)}$  and  $A_{\text{SL}}^{(2)}$ ,
        
$$c_{\mathcal{R}}[2] \leftarrow A_{\text{SL}}^{(1)}[4] \oplus A_{\text{SL}}^{(1)}[6] \oplus A_{\text{SL}}^{(1)}[8] \oplus A_{\text{SL}}^{(1)}[9] \oplus A_{\text{SL}}^{(1)}[13] \oplus A_{\text{SL}}^{(1)}[14],$$

        
$$c_{\mathcal{R}}[3] \leftarrow A_{\text{SL}}^{(1)}[4] \oplus A_{\text{SL}}^{(1)}[9] \oplus A_{\text{SL}}^{(1)}[10] \oplus A_{\text{SL}}^{(1)}[14] \oplus A_{\text{SL}}^{(1)}[15],$$

        
$$c_{\mathcal{R}}[4] \leftarrow A_{\text{SL}}^{(1)}[2] \oplus A_{\text{SL}}^{(1)}[5] \oplus A_{\text{SL}}^{(1)}[6] \oplus A_{\text{SL}}^{(1)}[8] \oplus A_{\text{SL}}^{(1)}[13] \oplus A_{\text{SL}}^{(1)}[15],$$

        
$$c_{\mathcal{R}}[5] \leftarrow A_{\text{SL}}^{(1)}[0] \oplus A_{\text{SL}}^{(1)}[6] \oplus A_{\text{SL}}^{(1)}[7] \oplus A_{\text{SL}}^{(1)}[8] \oplus A_{\text{SL}}^{(1)}[10] \oplus A_{\text{SL}}^{(1)}[13],$$

        
$$c_{\mathcal{R}}[6] \leftarrow A_{\text{SL}}^{(1)}[5] \oplus A_{\text{SL}}^{(1)}[7] \oplus A_{\text{SL}}^{(1)}[10] \oplus A_{\text{SL}}^{(1)}[11],$$

        
$$c_{\mathcal{R}}[7] \leftarrow A_{\text{SL}}^{(1)}[10] \oplus A_{\text{SL}}^{(1)}[11] \oplus A_{\text{SL}}^{(1)}[12] \oplus A_{\text{SL}}^{(1)}[15].$$

        
$$c_{\mathcal{R}}[8] \leftarrow A_{\text{SL}}^{(2)}[2] \oplus A_{\text{SL}}^{(2)}[8] \oplus A_{\text{SL}}^{(2)}[15],$$

        
$$c_{\mathcal{R}}[9] \leftarrow A_{\text{SL}}^{(2)}[1] \oplus A_{\text{SL}}^{(2)}[4] \oplus A_{\text{SL}}^{(2)}[15],$$

        
$$c_{\mathcal{R}}[10] \leftarrow A_{\text{SL}}^{(2)}[3] \oplus A_{\text{SL}}^{(2)}[6] \oplus A_{\text{SL}}^{(2)}[8],$$

        
$$c_{\mathcal{R}}[11] \leftarrow A_{\text{SL}}^{(2)}[4] \oplus A_{\text{SL}}^{(2)}[6] \oplus A_{\text{SL}}^{(2)}[12] \oplus A_{\text{SL}}^{(2)}[15],$$

        
$$c_{\mathcal{R}}[12] \leftarrow A_{\text{SL}}^{(2)}[8] \oplus A_{\text{SL}}^{(2)}[9] \oplus A_{\text{SL}}^{(2)}[12] \oplus A_{\text{SL}}^{(2)}[15].$$

7      $V[c_{\mathcal{R}}] \leftarrow v_{\mathcal{R}}$ ; /* There are  $2^8$  elements in  $V[c_{\mathcal{R}}]$  for each  $c_{\mathcal{R}}$  */
8   end
9   for  $c_{\mathcal{R}} \in \mathbb{F}_2^{8 \times 13}$  do
10     $L \leftarrow []$ 
11    for  $v_{\mathcal{R}} \in V[c_{\mathcal{R}}]$  do
12      Compute to the  $\blacksquare$  cells in  $A_{\text{DL}}^{(4)}$ , and one-byte  $End_{\mathcal{R}}$  for matching is
        derived by
13      
$$End_{\mathcal{R}} \leftarrow (A_{\text{DL}}^{(4)}[3] \oplus A_{\text{DL}}^{(4)}[4] \oplus A_{\text{DL}}^{(4)}[6] \oplus A_{\text{DL}}^{(4)}[8] \oplus A_{\text{DL}}^{(4)}[9])$$

14       $L[End_{\mathcal{R}}] \leftarrow v_{\mathcal{R}}$ 
15    end
16    for  $2^8$  possible values of  $A^{(1)}[3]$  do
17      Compute to the  $\blacksquare$  cells in  $A_{\text{DL}}^{(4)}$  and  $A_{\text{SL}}^{(4)}$ , derive one-byte  $End_{\mathcal{B}}$  for
        matching by
18      
$$End_{\mathcal{B}} \leftarrow (A_{\text{SL}}^{(4)}[0] \oplus A_{\text{DL}}^{(4)}[13] \oplus A_{\text{DL}}^{(4)}[14])$$

19      for  $v_{\mathcal{R}} \in L[End_{\mathcal{B}}]$  do
20        Reconstruct the (candidate) message  $X$ 
21        if  $X$  is a preimage then
22          Output  $X$  and stop
23        end
24      end
25    end
26  end
27 end
```